Performance Limits of Axial Turbomachine Stages

by

David Kenneth Hall

B.S.E., Duke University (2008)

Submitted to the Department of Aeronautics and Astronautics
in partial fulfillment of the requirements for the degree of

Master of Science in Aeronautics and Astronautics

at the

MASSACHUSETTS INSTITUTE OF TECHNOLOGY

February 2011

ARCHIVES

MASSACHUSETTS INSTITUTE OF TECHNOLOGY
FEB 25 2011
LIBRARIES

© Massachusetts Institute of Technology 2011. All rights reserved.

Author .....
Department of Aeronautics and Astronautics
December 17, 2010

Certified by.....
Edward M. Greitzer
H.N. Slater Professor of Aeronautics and Astronautics
Thesis Supervisor

Certified .....
Choon Sooi Tan
Senior Research Engineer
Thesis Supervisor

Accepted by .....
Eytan H. Modiano
Associate Professor of Aeronautics and Astronautics
Chair, Committee on Graduate Students

Performance Limits of Axial Turbomachine Stages

by

David Kenneth Hall

Submitted to the Department of Aeronautics and Astronautics
on December 17, 2010, in partial fulfillment of the
requirements for the degree of
Master of Science in Aeronautics and Astronautics

Abstract

This thesis assesses the limits of stage efficiency for axial compressor and turbine stages. A stage model is developed, consisting of a specified geometry and a surface velocity distribution with turbulent boundary layers. The assumptions and parameterization of the stage geometry allow for calculation of the magnitude of various loss sources in terms of eight input parameters. By (1) considering only the losses which cannot be eliminated (such as viscous dissipation within the boundary layer on wetted surface area), (2) selecting stage design variables for minimum loss, and (3) assessing performance in the incompressible limit, an upper bound on stage efficiency can be determined as a function of four stage design parameters. Under the given conditions, the maximum stage efficiencies are found to be 95.5% and 97.2% for compressor and turbine stages, respectively.

The results of the stage analysis are evaluated in the context of gas turbine generator and turbofan cycles for different levels of material and cooling technology. If the cycle temperature and pressure ratios are selected for minimum fuel consumption, even small increases in component efficiency can lead to substantial increases in overall engine efficiency. For example, if the efficiency of components is increased from 90% to 95% and the design is optimized, the specific fuel consumption of a gas turbine generator and turbofan engine are reduced by 17% and 19%, respectively. The stage level and cycle analyses carried out imply that component efficiency improvements leading to an appreciable increase in cycle thermal efficiency still remain to be realized.

Thesis Supervisor: Edward M. Greitzer
Title: H.N. Slater Professor of Aeronautics and Astronautics

Thesis Supervisor: Choon Sooi Tan
Title: Senior Research Engineer

Acknowledgments

First, I would like to thank my advisors, Professor Greitzer and Dr. Tan. For their guidance, enthusiasm, patience, and encouragement, both avising me in my research and teaching me in the classroom, I am extremely appreciative. Working with them has been a real pleasure. I'd also like to give special thanks to Professor Drela, whose guidance on the subjects of cascade aerodyanmics and boundary layers proved invaluable in development of the models used in the research, and Professor Cumpsty for his feedback and advice throughout the course of this research.

I am grateful for the support of the NASA Subsonic Fixed Wing N+3 project, which funded this research, as well as all those involved in the project. Thanks in particular to Sho Sato, Pritesh Mody, Dr. Elena de la Rosa Blanco, and Dr. Jim Hileman. Thanks also to Nathan Fitzgerald and George Kiwada at Aurora and Wes Lord and Professor Epstein at Pratt & Whitney for their technical insight.

My experience wouldn't have been complete without my interactions with the students of the Gas Turbine Lab. Whether collaborating on research, working together on problem sets and class projects, or just hanging out at social hour, I've been lucky to have good friends for colleagues. In particular, I'd like to mention Alex, Ben, Phil, and Arthur, with whom I shared the office of 31-257.

Thanks to Bill, Juan, and Leah; you guys are the best.

Last but certainly not least, I'd like to thank my family, without whom I never would have had the opportunity to come to a place like MIT and work on such an exciting project. Thanks Mom, Dad, Papa, and Christine for your love and support in this and in all my endeavors. I've been blessed to have been surrounded by people who have always believed in me, and for that I can't thank you enough.

Contents

1 Introduction **19**

1.1 Objectives 19

1.2 Previous work 20

1.3 Scope 22

1.3.1 Assumptions 22

1.3.2 Losses considered 23

1.3.3 Performance metrics 24

1.4 Contributions 24

1.5 Thesis outline 25

2 Performance Metrics and Loss Mechanisms **27**

2.1 Performance metrics 28

2.1.1 Adiabatic efficiency 28

2.1.2 Polytropic efficiency 29

2.1.3 Cycle efficiency 29

2.1.4 Specific fuel consumption 30

2.2 Second Law performance metrics 30

2.2.1 Flow availability 31

2.2.2 Rational efficiency 31

2.2.3 Rational cycle efficiency 33

2.3 Loss mechanisms 34

2.3.1 Boundary layer dissipation 34

2.3.2 Wake mixing 35

2.3.3 Injected or leakage flow mixing 36
2.4 Summary 37

3 Axial Turbomachine Stage Model **39**
3.1 Geometry 39
3.2 Velocity distribution 41
3.2.1 Compressor velocity distribution 41
3.2.2 Turbine velocity distribution 42
3.3 Loss Sources 43
3.4 Performance calculation 43
3.4.1 Overview of calculation procedure 43
3.4.2 Parametric dependence 44
3.4.3 Optimization of design variables 46
3.4.4 Design parameters 47
3.4.5 Presentation 48
3.5 Model Summary 48

4 Compressor Performance **49**
4.1 Baseline stage analysis 49
4.2 Optimized stage performance 50
4.3 Comparison to existing data 52
4.3.1 Dependence on flow and stage loading coefficients 52
4.3.2 Breakdown of loss sources 53
4.4 Effect of blade size 54
4.5 Summary of compressor stage performance 55

5 Turbine Performance **57**
5.1 Uncooled stage performance 57
5.2 Optimized stage performance 58
5.3 Comparison to existing data 60
5.3.1 Dependence on flow and stage loading coefficients 60

5.3.2 Breakdown of loss sources 60
5.4 Turbine efficiency and cooling flows 62
5.4.1 Efficiency as a measure of technology level 62
5.4.2 Efficiency as a cycle design parameter 62
5.5 Summary of turbine stage performance 63

6 Component Efficiency and Cycle Performance **65**
6.1 Simple gas turbine 65
6.2 Turbofan engine 68
6.3 Summary of cycle performance 70

7 Conclusion **71**
7.1 Summary 71
7.2 Conclusions 71
7.3 Future Work 72

A Boundary Layer Calculations **75**
A.1 Integral boundary layer formulation 75
A.1.1 Governing equations 75
A.1.2 Turbulent Closure 76
A.1.3 Leading edge treatment 76
A.2 Calculation procedure 77

B Tip Clearance Losses **79**
B.1 Clearance loss model 79
B.2 Clearance loss magnitudes 80
B.3 Comparison to existing methods and data 81

C Turbine Cooling **83**
C.1 Stage performance 83
C.1.1 Rational efficiency definition 84
C.1.2 Thermal mixing loss 84

C.1.3 Rational efficiency of a cooled stage 85
C.2 Cycle implications 87

D Turbomachine stage performance calculation procedure **91**
D.1 Flow angles 91
D.2 Camber lengths 92
D.2.1 Blade spacing 94
D.3 Velocity distribution 95
D.3.1 Turbine blade profile 96
D.4 Losses 98

E Cycle model **103**
E.1 Gas model 103
E.1.1 Gas properties 103
E.1.2 Gas mixture properties 104
E.1.3 Governing equations 104
E.2 State change calculations 105
E.2.1 Free stream quantities 105
E.2.2 Fan and compressor compression 106
E.2.3 Combustion 106
E.2.4 Mixing of two streams 107
E.2.5 Turbine expansion 108
E.2.6 Power turbine 108
E.2.7 Converging propelling nozzle 109
E.3 Performance calculation 110
E.3.1 Thermal efficiency 110
E.3.2 Thrust-specific fuel consumption 110

List of Figures

2-1 Enthalpy-entropy diagrams for compression and expansion processes . 28

2-2 Control volume (shown in red) used in downstream wake mixing loss calculation 35

2-3 Mixing of an injected flow 36

3-1 Meanline profiles and flow angles for compressor (top) and turbine (bottom) stages 40

3-2 Generic compressor blade velocity distribution 41

3-3 Generic turbine blade velocity distribution 42

3-4 Graphical summary of turbomachine stage efficiency calculation procedure 45

4-1 Smith chart, baseline compressor stage 50

4-2 Smith chart, optimized baseline compressor stage 51

4-3 Smith chart, one-dimensional correlation of Wright & Miller [45], reproduced from Dickens & Day [8] 52

4-4 Breakdown of losses at peak efficiency for the baseline compressor stage 53

4-5 Smith chart, small-bladed compressor stage 54

5-1 Smith chart, baseline uncooled turbine stage 58

5-2 Smith chart, optimized baseline uncooled stage 59

5-3 Turbine Smith chart based on experimental data, as produced in Mattingly [31] 60

5-4 Breakdown of losses at peak efficiency for the baseline uncooled turbine stage 61

6-1 Maximum gas turbine thermal efficiency vs component polytropic efficiency 66
6-2 Gas turbine thermal efficiency vs cycle pressure ratio, $\theta_t = 5.0$ 67
6-3 Turbofan thrust-specific fuel consumption vs component polytropic efficiency 69

B-1 Loss in efficiency per point in non-dimensional gap height as a function of stage loading and flow coefficients from 50% reaction compressor and turbine stages 80
B-2 Comparison of various tip clearance loss measurements and calculations 81

C-1 Exergy flow diagram for component with multiple incoming flows (a and b) producing work ($\dot{W}$) irreversibly ($\dot{I}$) and mixing (to state m) . 84
C-2 Smith chart, optimized cooled turbine stage 86
C-3 Breakdown of losses at peak efficiency for the optimized baseline cooled turbine stage 87
C-4 Optimal gas turbine temperature ratio as a function of allowable turbine metal temperature 88

List of Tables

3.1 Inputs to stage loss calculation procedure 45

4.1 Inputs for baseline compressor stage geometry 49
4.2 Inputs for rear compressor stage geometry 54

5.1 Inputs for baseline uncooled turbine stage geometry 58

6.1 Changes in engine performance with advances in various technology areas 69

C.1 Cooling input parameters for baseline cooled turbine stage 86
C.2 Component and cooling technology levels for optimum cycle temperature ratio calculation 88

Nomenclature

AR	blade aspect ratio
b	steady flow availability function ($= h - T_0 s$)
$C_{\mathcal{D}}$	dissipation coefficient
C_f	skin friction coefficient
c	chord
c_p	specific heat at constant pressure
c_v	specific heat at constant volume
DF	diffusion factor
F_N	net thrust
F_{sp}	specific thrust ($= F_N/\dot{m}_{\text{core}}$)
H	boundary layer shape factor ($= \delta^*/\theta$)
H^*	boundary layer kinetic energy shape factor ($= \theta^*/\theta$)
h	enthalpy, blade height
$\dot{I}$	rate of irreversibility ($= \dot{m} T_0 \Delta s$)
(LHV)	lower heating value
M	Mach number
$\dot{m}$	mass flow rate
P	power
$(PSFC)$	power-specific fuel consumption
p	pressure
$\dot{Q}_{\text{in}}$	rate of heat addition
Re	Reynolds number
s	entropy, blade pitch

T	temperature
$(TSFC)$	thrus-specific fuel consumption
u_e	boundary layer edge velocity
V	velocity
$\dot{W}$	power
Z	Zweifel coefficient
α	flow angle, fan bypass ratio
β	blade-relative flow angle
γ	ratio of specific heats $(= c_p/c_v)$
δ^*	boundary layer displacement thickness
ε	flow exergy
ϵ	exergetic effectiveness
ζ	injected flow mixing angle
η	efficiency
θ	boundary layer momentum thickness
θ^*	boundary layer kinetic energy thickness
θ_t	cycle stagnation temperature ratio $(= T_{t,\max}/T_{t,\min})$
Λ	stage reaction
ν	kinematic viscosity
ξ	boundary layer streamwise coordinate
π	pressure ratio
ρ	density
σ	solidity $(= c/s)$
τ	tip gap clearance, stagnation temperature ratio
Φ	dissipation
ϕ	flow coefficient $(= V_x/U)$
χ	mass flow fraction
ψ	stage loading coeffficient $(= \Delta h_t/U^2)$

Subscripts

c	compressor
f	fuel
o	overall
t	stagnation quantity, turbine
th	thermal
0	environmental state

Chapter 1

Introduction

Since its inception, the aerothermodynamic performance of the gas turbine engine has increased through higher cycle temperature and pressure ratios, enabled by increases in turbomachinery efficiency and improved material properties [27]. This thesis assesses limits of axial compressor and turbine efficiency and the effect of such limits on overall cycle performance. An axial turbomachine stage model is used to calculate local rates of entropy generation for those loss mechanisms that cannot be eliminated, such as skin friction on wetted surface areas. Cycle analyses are then carried out, with design variables optimized so that component efficiency is the only independent variable for cycle performance. This allows demonstration of the effect of advances in stage efficiency on cycle thermal efficiency or fuel consumption.

To the author's knowledge, no estimates of the performance limits based on the fundamental entropy-generating fluid processes within turbomachinery stages exist in the open literature. This thesis provides such estimates and allows evaluation of the upper limit of axial turbomachine stage efficiency as a function of a small number of stage design parameters.

1.1 Objectives

The objectives of this thesis are to evaluate, in a rigorous and consistent manner, the upper limit of axial turbomachine stage efficiency, and the effects of such levels of

performance on overall cycle efficiency. The main challenge in doing this is not in the calculations of the losses that occur, but rather the choices of which losses to consider, the conditions under which they should be evaluated, and the fidelity needed to provide useful information. These choices drove the development of a framework for evaluating turbomachine stage performance, making traceable assumptions representing advances in technology that may be possible in the future.

1.2 Previous work

Stage performance models

At the start, it seems useful to define the conceptual goals of the research. The aim is to evaluate the upper limit of performance rather than to produce results that match current machines. This is accomplished by focusing on losses that cannot be eliminated and selecting input parameters for minimum loss via standard optimization techniques. Turbomachine stage models that aim to realistically predict losses and trends for *current* technology, however, provide a framework from which such a loss model can be constructed. As one example, Koch & Smith [26] developed a model based on boundary layer calculations, calibrated to match experimental data, and with debits in efficiency calculated from individual loss sources. As a second example, Dickens & Day [8] developed a model to find the dependence of compressor stage efficiency on blade loading using boundary layer calculations on a simplified triangular velocity profile to calculate profile losses, an approach adopted in the current research.

Loss mechanisms in turbomachines

Loss mechanisms in turbomachine stages have been described in depth by a number of authors. Denton [7] provides an excellent source, listing correlations and calculations for most of the losses considered, and providing a starting point for the current research. A detailed examination of individual loss sources has been performed by Storer & Cumpsty [41], who provide a model for compressor tip clearance losses,

Yaras & Sjolander [47], who provide a similar model for turbine tip clearance losses, and Young & Wilcock [50], who provide a methodology for calculating the entropy generated by turbine cooling flows. There has not been, however, as far as the author is aware, any work in the open literature that builds a bottom-up loss model to estimate the limit of stage efficiency.

Cycle optimization

A number of procedures exist to define optimum cycle parameters for minimum fuel consumption. A basic method for picking optimum cycle temperature, pressure and bypass ratios for a turbofan engine is given by Cohen, Rogers, & Saravanamuttoo [37], although with component efficiencies assumed fixed. Guha [14] [15] explores gas turbine engine cycle optimization including real gas effects, but does not specifically target the effect of component efficiency on the overall cycle. The calculations described here treat the component efficiency as the independent variable, so advances in overall performance attributable to component design can be determined.

Exergy-based loss accounting

A useful tool in defining the "ideal" work needed to define stage or cycle efficiency is the thermodynamic quantity of *exergy*, the work that could be obtained by a system in a reversible process from a given state to a state of equilibrium with the environment. Exergy-based cycle analysis is now in wide use, particularly for complex power plants. Basic information on the subject is available in the literature [28] [33], and Clarke & Horlock [3] and Horlock [23] have presented exergy analyses for turbojet and turbofan engines. Exergy-based measures of efficiency are useful, since they provide a consistent measure of performance, regardless of state or the process in question. Horlock [20] explores exergy-based performance metrics for individual components, and the *rational efficiency* he describes is used in the present stage level analysis.

1.3 Scope

The issue of determining a meaningful upper bound on stage performance is framed by the assumptions made about the machine and the flows through it, the losses included in the analysis, and the metrics used to define performance. A brief discussion of these considerations is given here. The point to be emphasized is that the assumptions made bound the problem and drive the loss estimation process that follows.

1.3.1 Assumptions

Incompressibility

The flow is considered to be incompressible for the evaluation of mechanical dissipation. This assumption simplifies some of the calculations (such as the blade profile velocity distribution) and reduces the trade space of the analysis by eliminating Mach number as an input parameter. Compressibility effects have been found to decrease performance, either through increased dissipation in boundary layers or the presence of shocks [4] [29], and the incompressible flow behavior is thus viewed as an upper limit.

Turbulent boundary layers

A major source of entropy generation (loss) is viscous dissipation within boundary layers on the stage wetted area. The current analysis assumes fully turbulent boundary layers except for a small region of laminar flow in the accelerating boundary layer near the leading edge stagnation point (Appendix A outlines the calculation procedure for the growth of the profile boundary layer).

The evolution of the boundary layers is tied to the velocity distribution of the flow. The current analysis assumes generic velocity distributions on compressor and turbine blade profiles. The compressor has a triangular distribution with linearly decreasing suction side velocity; this closely matches the velocity distribution seen on real blades, and the adverse pressure gradient means that a fully turbulent boundary layer is an appropriate assumption for flows with high incoming turbulence intensity. The

turbine velocity profile is specified as rectangular, with constant velocity on both sides of the blade; while this does not closely resemble real turbine velocity distributions, it gives the lowest possible profile loss under the assumption of turbulent boundary layers.

In practice, large regions of laminar flow can exist, and the unsteadiness of the stage environment can effect the size of the laminar separation bubble and the location of transition from laminar to turbulent flow within the boundary layer [17] [19]. The dissipation in laminar boundary layers can be up to an order of magnitude smaller than in turbulent boundary layers, so that there is a decrease in total boundary layer loss roughly proportional to the fraction of the boundary layer that is laminar; this can account for stage efficiencies as much as a point higher than those presented in this thesis. The modeling of unsteadiness, laminar separation bubbles, and boundary layer transition are beyond the scope of this thesis, and the effect of laminar boundary layers is not considered.

Two-dimensional models

The magnitudes of losses are calculated using two-dimensional models. This allows the stage model to be characterized by a generic profile and annulus shape, and the entire geometry to be determined as a function of only eight stage parameters. Three-dimensional flow features are not modeled, however, this is consistent with the choices made about which losses to include: it is assumed that future designs will mitigate, or perhaps eliminate, the loss in performance due to three-dimensional effects.

1.3.2 Losses considered

Only losses associated with (1) skin friction on wetted solid surfaces, (2) the mixing out of wakes downstream of blades, and (3) mixing of tip leakage or injected flows are considered. These losses will remain regardless of future designs. Ignoring all other sources of entropy generation gives an upper limit on possible performance.

1.3.3 Performance metrics

At the stage level, the performance metric is the rational stage efficiency, which is defined in terms of thermodynamic exergy. In the incompressible limit, the rational, adiabatic, and polytropic efficiencies are equivalent. For the cycle-level calculations, the performance metric is thermal efficiency for the gas turbine cycle and thrust-specific fuel consumption for the turbofan engine; the gas and cycle models, as well as a description of the performance metrics are given in Appendix E. Aircraft level performance metrics are not considered, so the cycle design for minimum fuel consumption is a function of a specified temperature ratio, component efficiency, and a chosen fan pressure ratio. At both the stage and cycle level, only design point performance is examined.

1.4 Contributions

The contributions of this thesis are:

1. A methodology for calculating stage efficiency as a function of eight input stage parameters. A critical requirement for this methodology is a framework within which the losses are evaluated; these assumptions are such that the best-case scenario is targeted without reference to unrealistic advances.

2. Estimates for the limits of axial compressor and turbine stage efficiency for cases representative of aero engine gas turbine components, including behavior of optimal design variables.

3. A comparison of two different methods for evaluating the effect of turbine cooling flows. Second Law rational efficiency gives a consistent metric for evaluating the performance of a cooled turbine. It is argued, however, that the effect of cooling should be evaluated at the cycle level, since cooling requirements are tied to the choice of cycle temperature and pressure ratios, making *uncooled* turbine efficiency a more meaningful stage-level measure of technology level.

4. A definition of the trends in maximum gas turbine engine efficiency with increases in component performance, leading to an estimate of future increases in cycle efficiency directly attributable to advances in component design.

1.5 Thesis outline

Chapter 2 provides background information on performance metrics used in stage and cycle performance analyses, as well as descriptions of calculation procedures for the loss mechanisms considered. Chapter 3 gives a brief description of the axial turbomachine model used for the stage performance calculations, with a more detailed description of the calculations given in Appendix D. Chapters 4 and 5 present the results of the calculations for compressor and turbine stages, respectively (a discussion on cooled turbine stages is contained in Appendix C). Chapter 6 shows the effect of component performance on gas turbine engine efficiency, using a modular cycle model (described in detail in Appendix E). The summary and conclusions are given in Chapter 7.

Chapter 2

Performance Metrics and Loss Mechanisms

This chapter serves two purposes. One is to briefly defines conventional metrics for characteristic performance of turbomachine stages and gas turbine cycles before introducing the Second Law performance metrics to be used throughout the remainder of this thesis. Discussion of how these metrics relate to the conventional measures is given for context. A second is to describes calculation procedures for the four loss sources considered. In keeping with an exergy-based framework, expressions for mechanical dissipation (entropy generation) are given, rather than stagnation pressure loss.

Second Law performance metrics are used due to their applicability and consistency across various levels of performance analysis. Horlock [20] defines component performance metrics that can be used in a direct calculation of rational cycle efficiency. Drela [10] provides a framework where lost power, expressed as mechanical dissipation and evaluated at the blade row level translates directly to overall aircraft system performance.

As described in Chapter 1, incompressible flow is assumed in all calculations. Under this condition, the Second Law performance metrics are equivalent to adiabatic and polytropic efficiency for components with only one fluid stream (e.g. compressor and uncooled turbine stages).

2.1 Performance metrics

This section briefly describes the metrics that are most commonly used to characterize the performance of gas turbine engines and their components. More information on these metrics can be found in any of a number of texts on the subject, e.g. [5] [25] [37].

2.1.1 Adiabatic efficiency

The adiabatic efficiency is the ratio of the work needed (compressor) or obtained (turbine) for a reversible change in pressure to the actual work needed or obtained for the real process for the same change in pressure. Figure 2-1 shows enthalpy-entropy diagrams for compression and expansion processes.

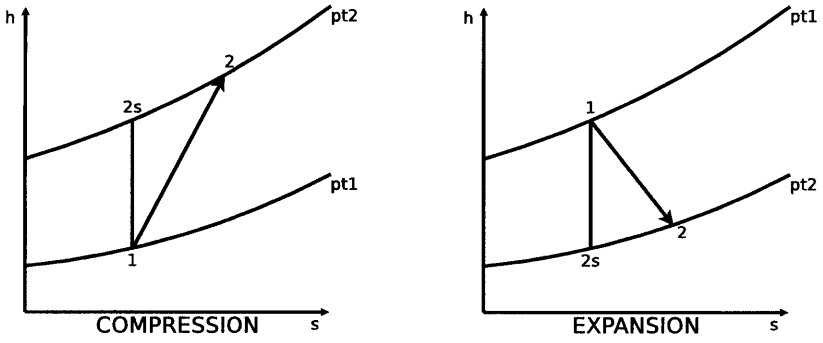


Figure 2-1: Enthalpy-entropy diagrams for compression and expansion processes

The efficiencies are given by

$$\eta_c = \frac{h_{t2s} - h_{t1}}{h_{t2} - h_{t1}}, \tag{2.1}$$

$$\eta_t = \frac{h_{t1} - h_{t2}}{h_{t1} - h_{t2s}}. \tag{2.2}$$

For a perfect gas[1] with constant specific heats (i.e. $\gamma = c_p/c_v$ is constant for the compression or expansion process), the adiabatic efficiency can be expressed in terms of pressure and temperature ratios as

$$\eta_c = \frac{\pi_c^{(\gamma-1)/\gamma} - 1}{\tau_c - 1}, \tag{2.3}$$

[1]The term "perfect gas" in this thesis refers to a gas that can be described by the state equation $p = \rho RT$ and whose energy is a function of temperature only.

$$\eta_t = \frac{1 - \tau_t}{1 - \pi_t^{(\gamma-1)/\gamma}}. \tag{2.4}$$

2.1.2 Polytropic efficiency

The adiabatic efficiency of a component depends on the pressure ratio over which it operates. To show the effect of technology in a way that is independent of pressure ratio, components are often characterized by a *polytropic efficiency*, defined as the efficiency for an infinitesimally small compression or expansion.

$$\eta_{\text{poly}} = \frac{\gamma - 1}{\gamma} \frac{dp_t}{p_t} \frac{T_t}{dT_t} \tag{2.5}$$

Using the Gibbs equation, the polytropic efficiency can be expressed as a measure of entropy generation.

$$\eta_{\text{poly}} = \left(1 - \frac{T_t ds}{dh_t}\right)^{\pm 1}, \tag{2.6}$$

where the exponent is $+1$ for compression and -1 for expansion.

2.1.3 Cycle efficiency

Gas turbine cycles can be characterized by the thermal efficiency, which is the ratio of the mechanical work obtained to the heat added.

$$\eta_{th} = \frac{\dot{W}}{\dot{Q}_{\text{in}}} \tag{2.7}$$

For open cycles with internal combustion, the heat added term can be replaced by the heating value of the fuel, (LHV). In the context of gas turbines for propulsion, the thrust power (i.e. the rate of work done by the engine) is the flight velocity V_∞ multiplied by the net thrust F_N, yielding the overall engine efficiency η_o.

$$\eta_o = \frac{F_N V_\infty}{\dot{m}_f (LHV)} \tag{2.8}$$

The overall efficiency can be expressed as the product of the engine thermal efficiency η_{th} and the propulsive efficiency η_{prop}. The first of these is the rate that kinetic energy

is added to the flow divided by the rate of fuel energy use

$$\eta_{th} = \frac{\dot{m}\Delta KE}{\dot{m}_f(LHV)}. \tag{2.9}$$

The propulsive efficiency η_{prop}, which relates the mechanical energy added to the flow to the thrust power delivered is given by

$$\eta_{\text{prop}} = \frac{F_N V_\infty}{\dot{m}\Delta KE}. \tag{2.10}$$

The expression for overall efficiency (2.8) does not provide a precise measure of engine efficiency, since (1) the concept of thrust becomes ambiguous for applications where the engine is highly integrated into the airframe [35], and (2) the heating value is not necessarily the appropriate measure of the available energy in the fuel, because the energy released assumes combustion at standard conditions.

2.1.4 Specific fuel consumption

Thrust engines are characterized by the thrust-specific fuel consumption ($TSFC$),

$$TSFC = \frac{\dot{m}_f}{F_N}, \tag{2.11}$$

This has units of mass flow per unit force (e.g. kg/N/s). $TSFC$ can be expressed in terms of overall engine efficiency, fuel heating value, and flight velocity, as,

$$TSFC = \frac{V_\infty}{\eta_o(LHV)}. \tag{2.12}$$

2.2 Second Law performance metrics

The use of exergy provides metrics for defining stage and cycle performance that are more rational measures of loss than above the conventional metrics [18] [28] [3] [23]. This section gives background information on exergy and the metrics to be used, with more detailed discussions available in the literature [1] [24] [28] [33].

Young & Horlock [50] argue that Second Law performance metrics have "the soundest thermodynamic foundation," since ideal work is defined as the work that could be obtained from a fully reversible process. Second Law metrics are particularly useful for components with multiple fluid streams, such as cooled turbines, where commonly used metrics such as adiabatic efficiency are not necessarily defined in a thermodynamically rigorous way. The stage performance metrics described here are adopted for the remainder of this thesis.

2.2.1 Flow availability

The steady flow availability function is given by

$$b = h_t - T_0 s, \tag{2.13}$$

where T_0 is the temperature of the environment in which the thermodynamic process or cycle operates. The flow exergy is given by

$$\varepsilon = b - b_0 = (h_t - h_{t0}) - T_0(s - s_0), \tag{2.14}$$

where h_{t0} and s_0 are the stagnation enthalpy and entropy of the environment, respectively. The exergy represents the maximum work that could be obtained through a reversible process starting at an initial state (h_t, s) and ending at the same state as the environment, state 0. At state 0, no more work can be extracted, since the flow is in equilibrium with the environment[2].

2.2.2 Rational efficiency

The change in exergy is the maximum amount of work that could be extracted between any two states. Comparing the useful work extracted to the decrease in exergy (or

[2]If the process involves a mixture of gases with different partial pressures than the same gases in the environment (e.g. a gaseous fuel is introduced and then combusted), additional terms arise due to the work that could be obtained as the flow moves from a solely physical equilibrium to physical *and* chemical equilibrium with the environment; this term is normally small for the applications being considered and is neglected here.

availability) gives the *exergetic effectiveness* ϵ:

$$\epsilon_c = \frac{\varepsilon_2 - \varepsilon_1}{h_{t2} - h_{t1}} = \frac{b_2 - b_1}{h_{t2} - h_{t1}} = \frac{h_{t2} - T_0 s_2 - h_{t1} + T_0 s_1}{h_{t2} - h_{t1}} = 1 - \frac{T_0(s_2 - s_1)}{h_{t2} - h_{t1}}, \tag{2.15}$$

$$\epsilon_t = \frac{h_{t1} - h_{t2}}{\varepsilon_1 - \varepsilon_2} = \frac{h_{t1} - h_{t2}}{b_1 - b_2} = \frac{h_{t1} - h_{t2}}{h_{t1} - T_0 s_1 - h_{t2} + T_0 s_2} = \left(1 - \frac{T_0(s_2 - s_1)}{h_{t2} - h_{t1}}\right)^{-1}. \tag{2.16}$$

Assuming $(1 - \eta) \ll 1$, the stage adiabatic efficiency can be approximated as

$$\eta \simeq \left(1 - \frac{T_{t2}(s_2 - s_1)}{h_{t2} - h_{t1}}\right)^{\pm 1}. \tag{2.17}$$

Comparison of Equation (2.17) to Equations (2.15) and (2.16) shows that both the exergetic effectiveness, also referred to as the *rational efficiency*, and the adiabatic efficiency measure the entropy generation due to irreversibility. The adiabatic efficiency multiplies the entropy generation by the final temperature, yielding a lost work for the process. The rational efficiency uses the environmental temperature T_0 to determine a lost work, which counts the actual lost work minus any newly created available work due to the fact that the fluid is now at a higher temperature than if the process had been isentropic.

Rational and adiabatic efficiencies

For components with a single stream, Equations (2.15) and (2.16) are sufficient to describe the exergetic effectiveness. The adiabatic efficiency can be related to the exergetic effectiveness as

$$\epsilon_c \simeq 1 - \frac{T_0}{T_{t2}}(1 - \eta_c), \tag{2.18}$$

$$\epsilon_t \simeq \frac{\eta_t}{\eta_t + \frac{T_0}{T_{t2}}(1 - \eta_t)}. \tag{2.19}$$

To obtain a numerical value for the effectiveness, an environmental state (with temperature T_0 and pressure p_0) must be defined. If the component is to be evaluated in the context of an overall cycle, the environmental state is defined as the state of the reservoir in which the engine operates (Horlock [20] discusses rational definitions for

component efficiencies in the context of a thermodynamic cycle). If the component effectiveness is to be evaluated without an overall cycle context, an appropriate analog to the environmental state must be chosen. From Equations (2.18) and (2.19), if the process exit state is taken as the environment, the effectiveness is approximately equal to the efficiency. If the reference state is taken to be the initial state for a compression process, the compressor effectiveness is a function of both efficiency and temperature ratio.

$$\epsilon_c = 1 - \frac{1 - \eta_c}{\tau_c} \tag{2.20}$$

For incompressible flows, the temperature ratio term τ_c is equal to unity, and the adiabatic efficiency, the polytropic efficiency, and the exergetic effectiveness of a compressor stage are equivalent. This is also true for an expansion process (turbine stage), where the reference state is usually taken as the exit state.

For components with multiple incoming or exiting flows, such as a cooled turbine, the expression for rational efficiency must be alterred to account for the exergy of each individual stream, and the rational and adiabatic efficiencies can no longer be simply related (see Appendix C).

2.2.3 Rational cycle efficiency

Rather than use the fuel heating value as a measure of the available energy in the fuel, we use the *chemical exergy* ε_{ch}, defined as the work that could be extracted if the fuel at a given state were burned with air at environmental conditions before bringing the products back into physical and chemical equilibrium with the environment [3] [28] [33]. Using an efficiency based on the fuel chemical exergy is appropriate because variations in the temperature or pressure of the fuel can result in heat release different from the fuel heating value. Fuel exergy also lends itself to use in well-to-wake analyses, where the system includes more than an engine cycle, and the fuel changes state (and therefore exergy) many times throughout the process. Following

the notation of Drela [10], the overall engine efficiency can be expressed as

$$\eta = \frac{P_K - \Phi_{\text{jet}}}{\dot{m}_f \varepsilon_{\text{ch}}}, \tag{2.21}$$

where P_K is the rate of mechanical energy addition to the flow passing through the engine, and Φ_{jet} is the viscous dissipation that occurs downstream in the exhaust jet.

2.3 Loss mechanisms

Irreversibility is a result of either viscous dissipation or heat transfer across a finite temperature difference. Heat transfer across a finite temperature difference can occur during mixing, where two fluid streams start at different temperatures.

Within an axial turbomachine stage, these loss sources can be described in terms of three fluid phenomena:

1. viscous dissipation within boundary layers on blades and passage walls,
2. mixing out of viscous wakes downstream of blade rows, and
3. mixing of an injected or leakage flow with the bulk main flow.

2.3.1 Boundary layer dissipation

Most of the viscous dissipation in a turbomachine stage occurs within the viscous regions on the blades and endwalls. The dissipation that occurs in a 2D flow on a surface of unit span can be expressed in terms of the boundary layer kinetic energy thickness θ^* [10]:

$$\Phi(\xi) = \frac{1}{2}\rho u_e^3 \theta^*(\xi) = \int_0^\xi \rho u_e^3 C_{\mathcal{D}} d\xi, \tag{2.22}$$

where $C_{\mathcal{D}}$ is a *dissipation coefficient*, and ξ is the distance along the blade surface.

Correlations for the dependence of $C_{\mathcal{D}}$ on the state of the boundary layer show that for the range of Reynolds numbers encountered in turbomachine stages (Re $\sim 10^6$), if the boundary layer shape factor $H = \delta^*/\theta$ is low (i.e. the boundary layer is not close to

separation) the dissipation coefficient can be approximated as constant [7] [11]. If so, combined with the assumption of incompressibility, the dissipation can be expressed simply in terms of the flow velocity distribution at a solid surface $\mathcal{S}$:

$$\Phi = \rho C_{\mathcal{D}} \iint u_e^3 d\mathcal{S} \tag{2.23}$$

2.3.2 Wake mixing

The dissipation that occurs in the mixing out of a viscous wake downstream of a row of airfoils can be estimated from continuity, momentum, and energy conservation for the control volume shown in Figure 2-2, assuming the static pressure and flow angle

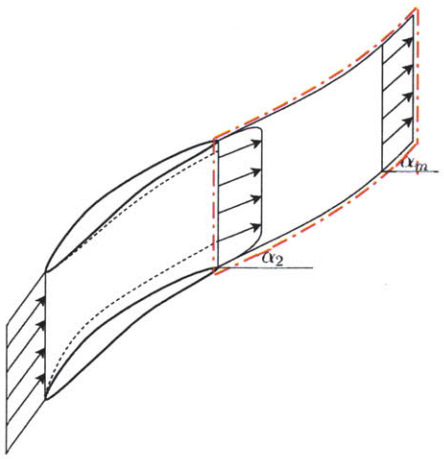


Figure 2-2: Control volume (shown in red) used in downstream wake mixing loss calculation

are uniform across the exit plane of the blade row. The mixed out flow angle α_m and static pressure drop $(p_m - p_2)$ can be found in terms of the blade exit angle α_2 and the trailing edge boundary layer properties (δ^*, θ, and θ^*). The dissipation that occurs in the mixing process is equal to the difference between the flux of mechanical energy (kinetic energy plus potential energy due to pressure) entering and exiting the

control volume.

$$\frac{\Phi}{\dot{m}V_2^2} = \cos^2\alpha_2\left(1-\frac{\delta^*}{W\cos\alpha^2}\right)\left[\frac{\theta}{W\cos\alpha_2}-\left(1-\frac{\delta^*}{W\cos\alpha_2}\right)+\left(1-\frac{\delta^*}{W\cos\alpha_2}\right)^2\right]$$
$$+\frac{1}{2}\left[1-\frac{\delta^*}{W\cos\alpha_2}-\frac{\theta^*}{W\cos\alpha^2}-\left(\frac{\cos\alpha_2}{\cos\alpha_m}\right)^2\left(1-\frac{\delta^*}{W\cos\alpha_2}\right)^3\right] \tag{2.24}$$

2.3.3 Injected or leakage flow mixing

Entropy generation also occurs due to mixing of injected or leakage flow into the main flow. Figure 2-3 shows a control volume for a two-dimensional mixing analysis. It is assumed the static pressure of the injected flow is equal to the static pressure at the entrance of the control volume.

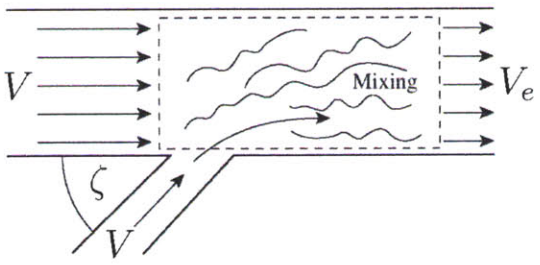


Figure 2-3: Mixing of an injected flow

The mechanical dissipation is equal to the difference between the flux of mechanical energy entering and exiting the control volume, and is given by

$$\frac{\Phi}{\dot{m}V_e^2} = \left[\frac{2\chi-\chi\cos\zeta}{1+\chi}\right]-\left[\frac{\chi^2+2\chi}{2(1+\chi)^2}\right], \tag{2.25}$$

where χ is the ratio of injected mass flow to incoming mainstream mass flow.

If the relative mass flow of the injected flow is small ($\chi \ll 1$), it can be assumed the mixing happens with negligible change in the velocity or pressure of the main flow and the dissipation is equal to the kinetic energy of the injected flow *in the frame of reference of the main flow*, which is lost as the injected flow equilibrates with the main flow.

$$\frac{\Phi}{\dot{m}V_e} = \chi(1-\cos\zeta) \tag{2.26}$$

2.4 Summary

This chapter has described the loss mechanisms considered and the accounting methods used to keep track of them. These loss mechanisms and performance metrics are the foundation for the stage loss model and efficiency calculations that follow.

The power-based rational efficiency is chosen as the performance metric for all stage-level efficiency calculations, but in the incompressible limit considered, this is equivalent to the adiabatic and polytropic efficiencies. Procedures for calculation of the magnitudes of various sources of entropy generation have been summarized.

Chapter 3

Axial Turbomachine Stage Model

This chapter describes the estimation of turbomachine stage losses. Generic stage geometries and surface velocities are parameterized by eight inputs, allowing the losses presented in Section 2.3 to be determined relative to the stage work and giving debits in stage efficiency due to each individual loss mechanism. The losses can then be combined to give an estimate of the overall stage efficiency.

Values of some of the inputs, for example solidity and reaction, can be selected to minimize losses. The efficiency has a monotonic dependence on the others, and these must be chosen based on additional design considerations. The optimization of design variables for minimum loss gives an estimate for the maximum stage efficiency as a function of four stage design parameters[1]. The compressor and turbine stage models are described in parallel, since many features of the calculations are the same for both, even though the assumed flow turning and assumed blade geometries and velocity distributions are different.

3.1 Geometry

Compressor and turbine stages are assumed to consist of one row of rotating blades (rotors) followed by one row of stationary vanes (stators); inlet guide vanes are not

[1]The optimized stage efficiency can be determined in terms of Reynolds number, aspect ratio, hub-to-tip radius ratio, and non-dimensional gap height.

included in the loss estimates. Flow angles are given in both stationary (α) and rotor-relative (β) frames, with subscripts indicating station numbers: 1 upstream of the rotor, 2 between the rotor and stator, 3 downstream of the stator. A repeating-stage design is assumed, that is the flow angles at the exit of a stage are equal to the flow angles at the inlet. A two-dimensional analysis is used with the rotor assumed to be moving at a mean velocity $U = \omega r$, where ω is the rotation rate of the rotor and r is the profile radius, taken here as the mean radius.

The stage geometry is described by the solidity $\sigma = c/s$, where c is the blade chord, and s is the spacing between blades (taken at the meanline radius), the aspect ratio $AR = h/c$ and the hub-to-tip ratio $r_r = r_{\text{hub}}/r_{\text{tip}}$. A gap is assumed to exist between the rotor blade tip and the engine casing, characterized by the gap-to-height ratio τ/h. Compressor airfoils are modeled as having circular arc camber lines, while the camber of turbine airfoils is parabolic. Effects on the blade span are assumed to be captured by the two-dimensional blade profile, so no further details of the blade geometry are necessary.

Figure 3-1 shows generic meanline stage profiles with accompanying velocity triangles for a compressor and turbine stage.

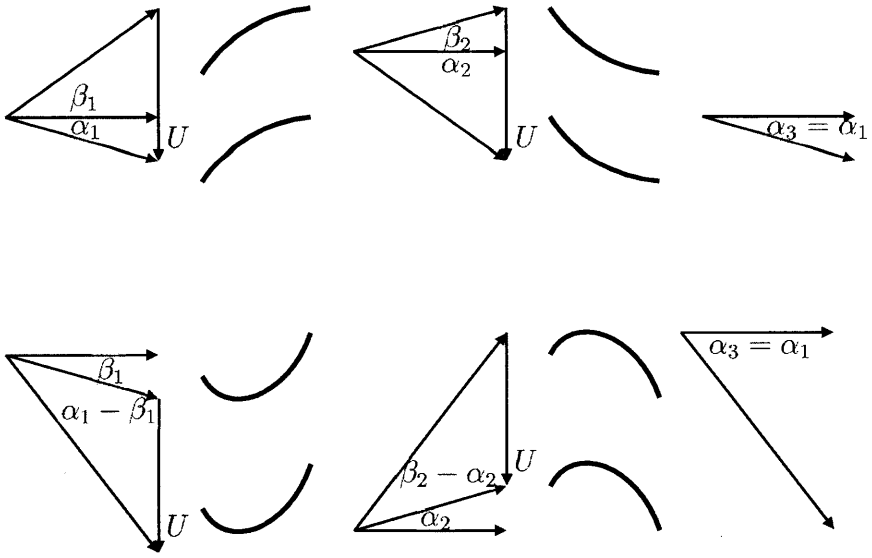


Figure 3-1: Meanline profiles and flow angles for compressor (top) and turbine (bottom) stages

3.2 Velocity distribution

3.2.1 Compressor velocity distribution

A triangular velocity distribution, similar to that used by Dickens and Day [8], is assumed (See Figure 3-2). Flow enters at $V_1 = V_x/\cos\alpha_{\text{in}}$ where α_{in} is the blade-relative inlet flow angle (β_1 for the rotor, α_2 for the stator), has leading edge velocities of $V_1 \pm \Delta V$ on the upper and lower surfaces, and has linear deceleration (or possible acceleration on the pressure side) to $V_2 = V_x/\cos\alpha_{\text{in}}$. On the endwalls, the velocity is taken as increasing linearly from pressure side velocity to suction side.

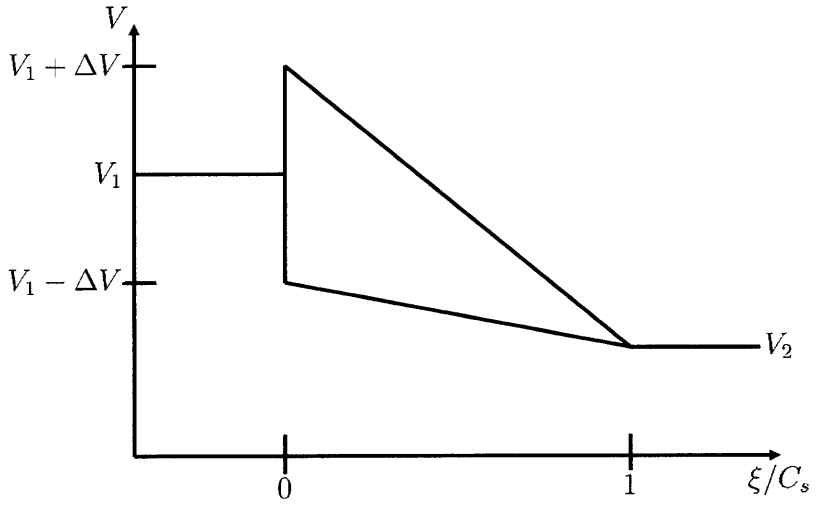


Figure 3-2: Generic compressor blade velocity distribution

This velocity distribution has been shown to closely approximate computational results for low-speed compressor cascades [8]. It captures the leading edge velocity difference, where the pressure and suction side velocity jumps can be approximated as equivalent if the blades are thin and have small camber. It also captures a continuous deceleration towards the blade row exit velocity on the suction side, which drives the turbulent boundary layer growth.

3.2.2 Turbine velocity distribution

For turbines, a rectangular velocity distribution, as presented by Denton [7], is used (See Figure 3-3). The velocity on each side of the blade is given by $\overline{V} \pm \Delta V$, where $\overline{V}$ is an average velocity. The magnitude of ΔV can be calculated from the circulation for a single blade passage, and $\overline{V}$ can be found in terms of ΔV using conservation of angular momentum (see Appendix D). As in the compressor, the endwall velocity is taken to increase linearly from pressure side to suction side.

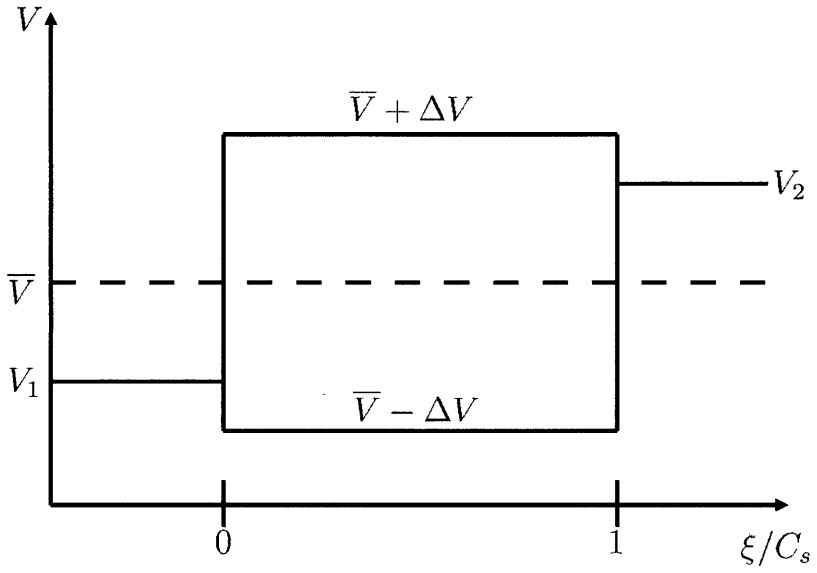


Figure 3-3: Generic turbine blade velocity distribution

The velocity distribution in Figure 3-3 gives the minimum attainable blade surface dissipation if a constant dissipation coefficient is assumed (a reasonable assumption for turbulent flow, since the pressure gradient is not adverse and the boundary layer shape factor is low). In the compressor, the rate of deceleration drives the boundary layer growth and associated loss. In the turbine, the profile loss is driven by overspeed regions, where $C_D u^3$ is large. The rectangular velocity does not closely approximate actual turbine cascade velocity distributions, but it captures the trends in overspeeds ($V + \Delta V$ in this case) as a function of turning and blade spacing.

3.3 Loss Sources

The losses considered are profile losses (boundary layer dissipation on the blade and vane surfaces and the mixing out of the wakes downstream), endwall (hub and casing or shroud) boundary layer dissipation, and tip clearance losses.

The profile losses are calculated in terms of trailing edge boundary layer properties. These are found using an integral boundary layer calculation [11] with the blade velocity of section 3.2. The endwall losses are calculated using the specified velocity distribution and a constant dissipation coefficient.

Rotor tip clearance losses for both compressor and turbine stages are estimated using the mixing analysis for unshrouded blades presented by Denton [7].[2] The size of the tip clearance gap can be fixed or varied to explore the effect of clearance size on stage efficiency.[3]

3.4 Performance calculation

With the assumptions for the stage geometries and flow characterization, the magnitudes of the various losses within the stage and the resulting stage efficiency can be found as functions of eight of stage parameters. Some of these inputs have values which minimize losses. Optimizing them allows for an estimate of maximum attainable stage efficiency as a function of only four stage design parameters.

3.4.1 Overview of calculation procedure

The meanline profile geometry is characterized by the flow coefficient $\phi = V_x/U$, the stage loading coefficient $\psi = \Delta h_t/U^2$, the inter-stage swirl angle α_1, and the solidity

[2]Storer & Cumpsty [41] and Yaras & Sjolander [47] present similar mixing analyses with various assumptions (see Appendix B). Denton's method is used in the present calculations because it gives an estimate for the minimum tip clearance loss based on the fundamental entropy-generating process (mixing of the clearance flow with the main flow on the blade suction side) without any knowledge or assumptions about the details of the flow near the blade tip.

[3]The current model gives minimum loss at zero clearance. In practice, this would lead to corner separation, and minimum loss is typically observed at non-zero clearance (Cumpsty [4] gives a discussion on optimal tip clearance heights).

$\sigma = c/s$. The flow angles and velocity triangles can be calculated in terms of the flow coefficient, stage loading coefficient, and the inter-stage swirl, which can be chosen to satisfy a specific degree of reaction. The blade spacing is characterized by the solidity, which can be specified or chosen to satisfy a specified diffusion factor (for a compressor blade row) or Zweifel coefficient (for a turbine row).

The annular geometry (namely the area of the endwalls relative to the mass throughflow area) is set by specification of blade aspect ratio $AR = h/c$ and hub-to-tip radius ratio $r_{\text{hub}}/r_{\text{tip}}$. The rotor tip clearance is characterized by a gap-to-height ratio τ/h.

The blade shape and surface area are calculated using the assumed camber. With geometry and the velocity triangles known, blade and endwall surface velocities can be determined using the velocity profiles described. The two-dimensional turbulent integral boundary layer method described in Appendix A is used to calculate the blade surface dissipation, with the wake mixing dissipation found from a control volume analysis. The endwall boundary layer dissipation is calculated using a constant dissipation coefficient ($C_{\mathcal{D}} = 0.002$). The losses due to mixing of rotor tip clearance flows are determined using a control volume analysis for two-dimensional mixing of two streams. Figure 3-4 gives a graphical summary of the calculation procedure, with a detailed discussions given in Appendix D.

3.4.2 Parametric dependence

The stage efficiency can be calculated from the sum of the various efficiency debits $\Delta\eta$ corresponding to each loss mechanism (e.g. boundary layer dissipation or mixing), assuming $\Delta\eta \ll 1$.

$$\eta_{\text{stage},c} = 1 - \sum \Delta\eta \tag{3.1}$$

$$\eta_{\text{stage},t} = \left(1 + \sum \Delta\eta\right)^{-1} \tag{3.2}$$

The final result for stage efficiency is dependent on the inputs listed in the previous section and reproduced in Table 3.1. For purposes of presentation, the stage loading

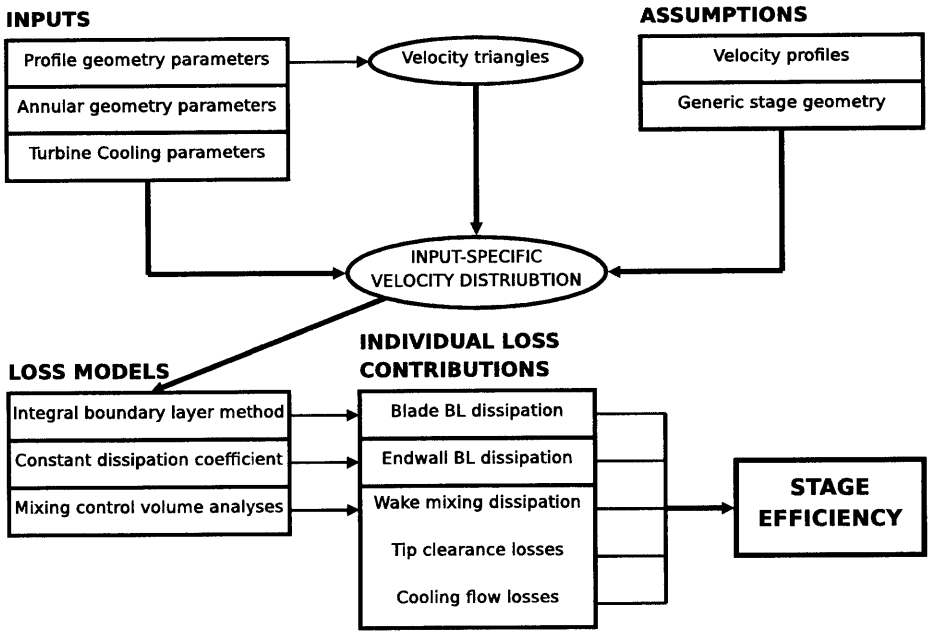


Figure 3-4: Graphical summary of turbomachine stage efficiency calculation procedure

Flow coefficient	$\phi = V_x/U$	independent
Stage loading coefficient	$\psi = \Delta h_t/U^2$	independent
Aspect ratios	$AR = h/c$	design parameters
Hub-to-tip ratios	$r_{\text{hub}}/r_{\text{tip}}$	design parameters
Gap-to-height ratio	τ/h	design parameter
Inter-stage swirl	α_1	design variable
Solidities	$\sigma = c/s$	design variables

Table 3.1: Inputs to stage loss calculation procedure

and flow coefficients are taken as independent variables.

With the assumptions used, the stage efficiency has a monotonic dependence on aspect ratio, hub-to-tip radius ratio, and Reynolds number. These three parameters are considered *design parameters* which are fixed for a given stage type. The remaining quantities (solidities and inter-stage swirl) are *design variables*, with optimal values which maximize stage efficiency as a function of the independent variables and design parameters.

3.4.3 Optimization of design variables

To find the limit on stage efficiency, the design variables are optimized as a function of the independent variables and design parameters. This is done using the built-in MATLAB® optimization routine `fminsearch`. The downhill simplex method [34] [36] on which this function is based is well-suited for this particular problem because there are only three design variables (α_1, σ_{rotor}, and σ_{stator}) and because it does not require calculation of the gradient of the objective function (stage efficiency in this case) with respect to the design variables. The initial guesses needed for optimization of inter-stage swirl and solidity are obtained from conventional choices of stage reaction, diffusion factor, and Zweifel coefficient.

Inter-stage swirl

Choice of the inter-stage swirl angle, α_1 sets the *degree of reaction*, the ratio of rotor static enthalpy rise to the stage enthalpy rise. While real turbomachine stages may be designed with a range of reactions [4], a degree of reaction close to 0.5 (when stage static pressure rise is divided evenly between the rotor and stator) produces blade boundary layers with the smallest profile losses [25]. With the generic blade velocity profile, a degree of reaction of 50% maximizes profile efficiency, as it minimizes the peak velocity of the stage, which drives the entropy generation (since the loss is nearly proportional to the quantity $\int u^3 d\xi$).

Compressor solidities

The issue of blade spacing brings about an interesting tradeoff. Blades with high solidities (small spacing) will have relatively flat velocity profiles, leading to small profile losses, but a larger number of blades. Low solidity blades will have a large dissipation per blade and are more prone to separation, but there are fewer of them. Historically, the *diffusion factor* has been used to pick appropriate compressor blade spacing given the bladerow flow angles. Experiments have shown that for diffusion factors above 0.45, the boundary layer approaches separation, with large losses, eliminating the

advantage of a small number of blades [25].

Turbine solidities

The favorable overall pressure drop present in turbine stages means that separation is only an issue if the suction side has large overspeeds. The *Zweifel coefficient* is a measure of how closely the pressure distribution approaches a constant value on each side of the blade, with the pressure side equal to the upstream stagnation pressure. A solidity corresponding to a Zweifel coefficient near 1 is sometimes cited as a good choice for a given blade design [25], but it has been shown that Zweifel coefficients as high as 1.5 may be optimal [6].

3.4.4 Design parameters

The calculated efficiencies have a monotonic dependence on input Reynolds number, aspect ratio, hub-to-tip ratio, and non-dimensional gap height. In practice, these quantities may be chosen based on effects not captured or considered by the current model. For compressors it has been observed that low aspect ratios are desirable, due to aerodynamic performance, stability, and structural considerations [42]. For turbines, aspect ratio may be limited by allowable blade stresses [25]. For a given machine, mass flow and Reynolds number will be fixed, and hub-to-tip ratio may be chosen for a desired tip Mach number. Tip clearance is constrained by machining and structural capabilities. The current model has minimum loss at zero clearance, but again, it is observed that non-zero gap heights appear to be optimal due to the presence of corner separation at zero clearance [4].

In the calculations that follow, the inputs are fixed to represent various types of aero engine turbomachine stages[4]. The variations in efficiency with changes in the design parameters are due to changes in the surface area per blade passage, to which the losses are nearly proportional. The current model should thus not be used outside

[4]Results for first and last high pressure compressor stages are presented in Chapter 4, a low pressure turbine stage is presented in Chapter 5, and a cooled high pressure turbine stage is presented in Appendix C.

this range of representative cases because effects not considered or not captured by the two-dimensional loss models may become important.

3.4.5 Presentation

Results of the calculations will be presented as *Smith charts*: contour plots of stage efficiency versus flow coefficient and stage loading coefficient. The reasoning behind this becomes clear upon inspection of the input variables of the calculation: the blade aspect ratio, hub-to-tip ratio, gap height ratio, and cooling parameters (in the case of a cooled turbine stage) are fixed for a given stage type or location, and the inlet flow angle and solidities can be optimized as described. The flow coefficient and stage loading coefficient can thus be considered the only remaining independent variables, the choice of which will ultimately determine the number of stages required for a given pressure rise.

3.5 Model Summary

A model has been described for estimating axial turbomachine stage losses. Using generic geometries and velocity distributions and optimizing stage design variables, the losses can be determined in terms of four inputs. In Chapters 4 and 5, the results of the model are shown as estimates for the upper limits on performance.

Chapter 4

Compressor Performance

This chapter presents the findings on compressor stage performance based on the calculations outlined in Chapter 3. Optimization of the design variables – given either as a diffusion factor and degree of reaction or blade solidities σ_r and σ_s and inter-stage swirl angle α_1 – allows for definition of maximum stage efficiency as a function of stage loading and flow coefficients, blade aspect ratio, hub-to-tip ratio, non-dimensional tip clearance height, and Reynolds number.

4.1 Baseline stage analysis

A compressor stage meant to represent the first stage of an aero engine high pressure compressor [16] is used as a baseline case for the discussion. The inputs are listed in Table 4.1, and the performance is plotted in Smith chart form in Figure 4-1. A peak

Reynolds number	$\mathrm{Re}_c = V_x c/\nu$	500,000
Aspect ratios	$A_r = h/c$	2.25
Hub-to-tip ratios	$r_{\mathrm{hub}}/r_{\mathrm{tip}}$	0.65
Gap-to-height ratio	τ/h	0.01
Degree of reaction	Λ	0.5
Diffusion Factor	DF	0.45

Table 4.1: Inputs for baseline compressor stage geometry

stage efficiency of 95.5% is observed. This is a substantial improvement over current

state-of-the-art compressors, which have polytropic efficiencies around 92% [2]. The large white area in the top-left corner (low flow coefficient and high stage loading) represents conditions that result in separation of the boundary layer on the blade surface. At these high loadings, even with high solidity to reduce the diffusion factor, the deceleration of the flow leads to separation.

The existence of a region of peak efficiency implies that at lower loadings, stage work increases faster than losses as the loading increases. Closer to separation, however, the dissipation within the boundary layer near the trailing edge of the blade increases rapidly with loading, and efficiency drops. This agrees with the findings of Dickens and Day [8], who concluded that increasing stage loading above that of conventional designs (0.2 to 0.4) led to higher profile loss.

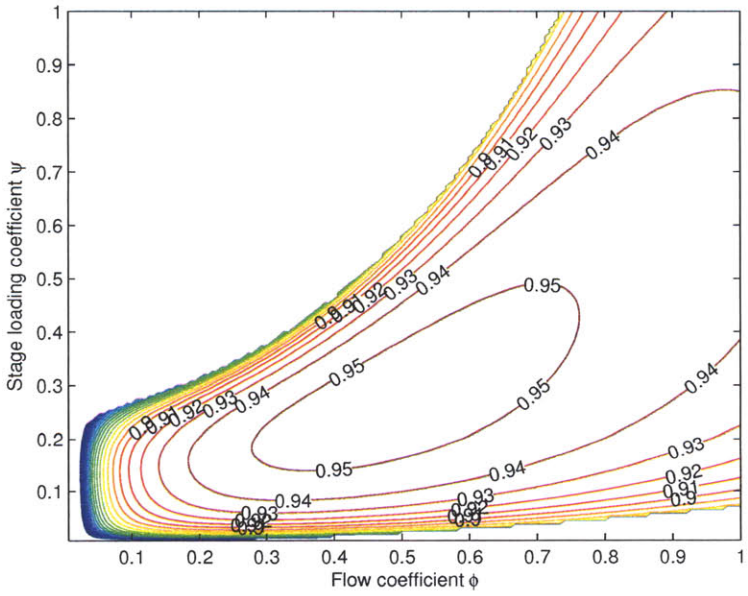


Figure 4-1: Smith chart, baseline compressor stage

4.2 Optimized stage performance

As discussed in Chapter 2, the blade spacing and incoming flow angle can be optimized for maximum stage efficiency. Figure 4-2 shows the Smith chart with optimized

reaction and diffusion factor. The location and magnitude of the peak efficiency do

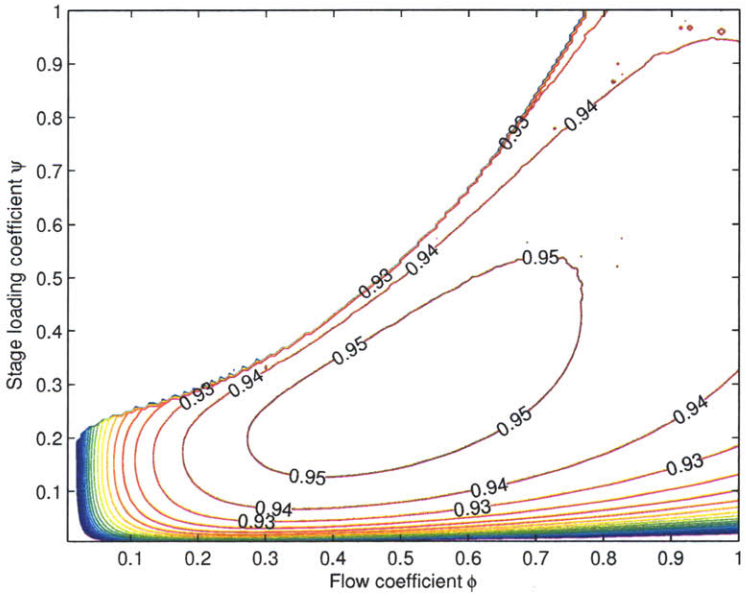


Figure 4-2: Smith chart, optimized baseline compressor stage

not change appreciably from the baseline case. The main difference between baseline and optimized cases is the smaller gradient of efficiency in the high efficiency region for the optimized case.

For low stage loading coefficient (less than 0.2, say), peak efficiency occurs at low values of diffusion factor (around 0.4) and high values reaction (near 80%). As the stage loading is increased and flow coefficient is decreased (increased turning), optimal diffusion factor increases and reaction decreases. At the separation limit, maximum efficiency occurs at a diffusion factor near 0.5 and a reaction near 50%. The efficiency is insensitive to these design variables however, as seen from the small change in efficiency after optimization, especially at the location of maximum efficiency. The choices of reaction and diffusion factor used in the baseline case are thus appropriate for illustrating the behavior of peak efficiency as a function of the stage design parameters.

4.3 Comparison to existing data

4.3.1 Dependence on flow and stage loading coefficients

Figure 4-3 shows a partial Smith chart by Dickens & Day produced using a one-dimensional correlation [8]. Comparison with Figure 4-1 shows similar trends in

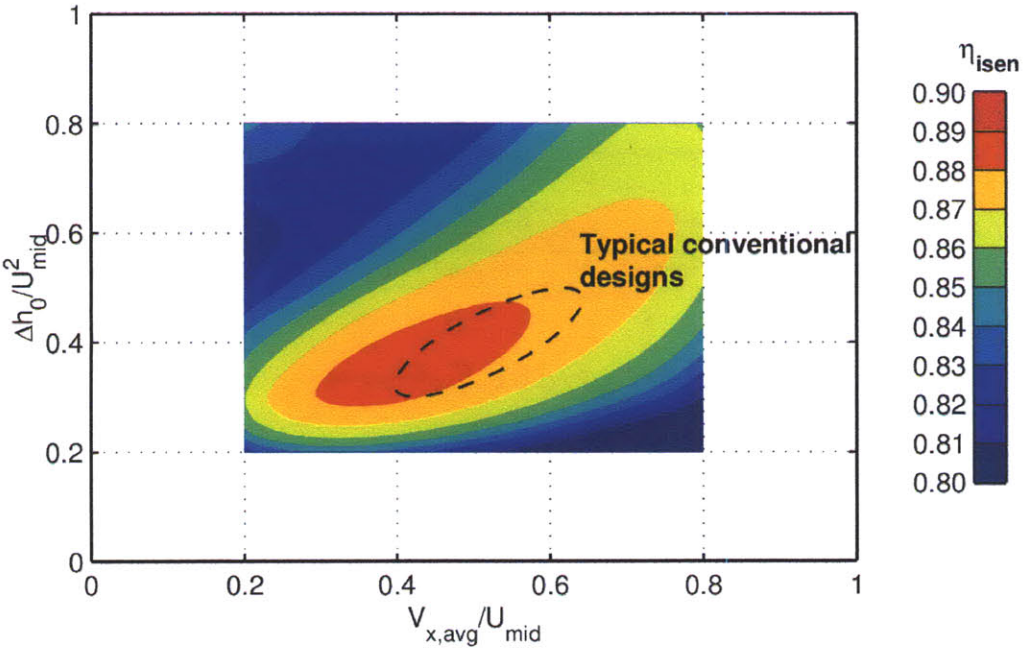


Figure 4-3: Smith chart, one-dimensional correlation of Wright & Miller [45], reproduced from Dickens & Day [8]

efficiency between the correlation and loss model described in this thesis. For both, a peak efficiency exists at a stage loading coefficient near 0.3 and a flow coefficient around 0.4. The main difference between the two is the magnitudes of the efficiencies: the correlation gives efficiencies approximately 5% lower than the loss model. This is expected, since the correlation is based on historic performance, while the loss model represents an upper limit of attainable performance.

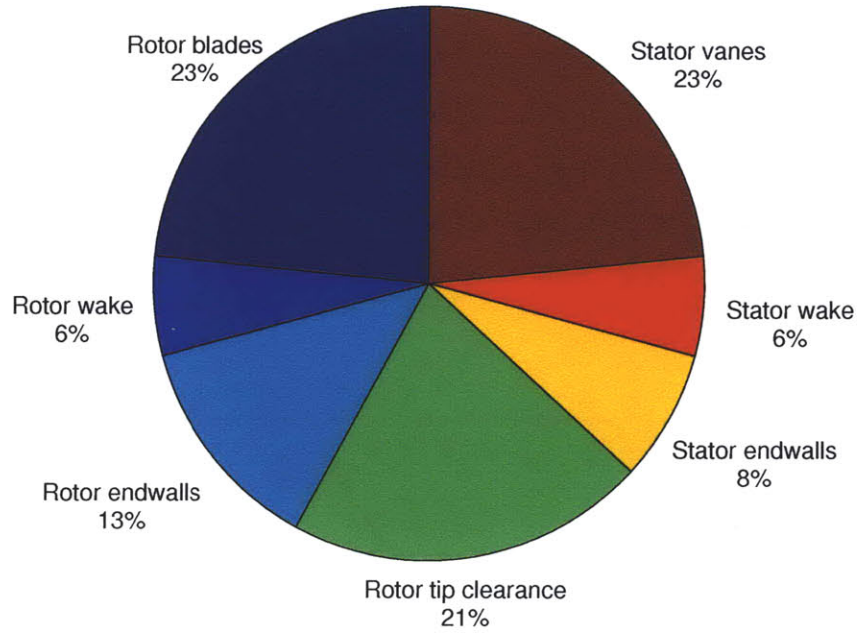


Figure 4-4: Breakdown of losses at peak efficiency for the baseline compressor stage

4.3.2 Breakdown of loss sources

Figure 4-4 shows the relative magnitudes of the seven individual loss sources considered for the baseline stage. There is an even split between rotor and stator profile losses because of the choice of 50% reaction. The endwall losses in the rotor are larger than in the stator because the velocity on the casing is higher than in the blade-relative frame. For each blade row, the downstream wake mixing loss is 20% of the total profile loss. The tip clearance loss is about 20% of the total stage loss for a gap to blade height ratio of 0.01; this corresponds to a loss of one percent in stage efficiency for each percent increase in non-dimensional blade height.

4.4 Effect of blade size

A major challenge of designing engines with high pressure ratios (leading to high thermal efficiency) is design of rear stages with small blade heights and large non-dimensional tip gap clearances, high hub-to-tip radius ratios, and low aspect ratios.

To show the effect of blade size, a case representing the rear stage of the same machine considered for the baseline case is given in Figure 4-5. The inputs are listed in Table 4.2. The degree of reaction and diffusion factor have been optimized at each point.

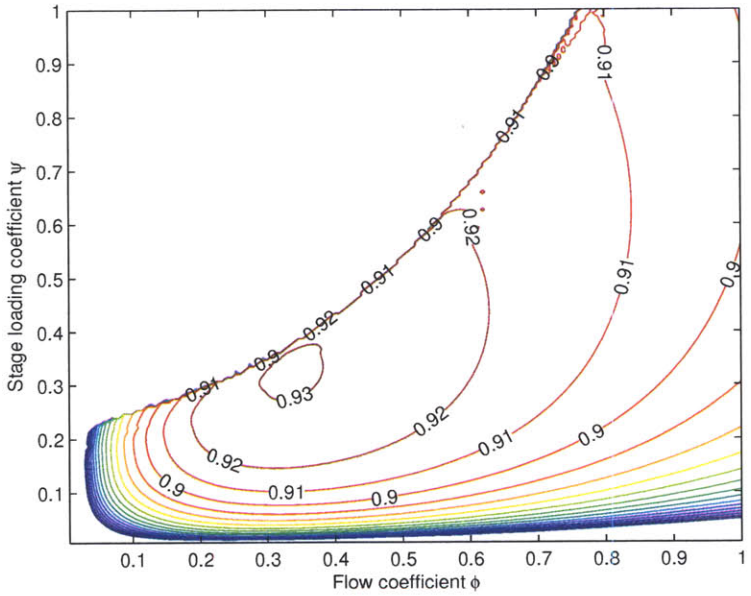


Figure 4-5: Smith chart, small-bladed compressor stage

Reynolds number	$\mathrm{Re}_c = V_x c/\nu$	1,000,000
Aspect ratios	$A_r = h/c$	1.25
Hub-to-tip ratios	$r_{\mathrm{hub}}/r_{\mathrm{tip}}$	0.9
Gap-to-height ratio	τ/h	0.05

Table 4.2: Inputs for rear compressor stage geometry

Most of the trends are similar to those seen with the baseline case, but the efficiency is at least 1.5 points lower over the entire range: the peak efficiency of 93.1%

occurs at a flow coefficient of 0.3 and stage loading coefficient of 0.3, and decreases faster away from the peak than the baseline case.

The lower aspect ratio contributes to greater loss, since the total wall area relative to the mass flow area (a ratio to which the loss is nearly proportional) grows with a decrease in aspect ratio for similar stages. A lower dissipation coefficient due to lower Reynolds number slightly decreases the profile loss.

The main factor contributing to decreased efficiency is the larger relative gap height. For the range of design parameters considered, the tip clearance loss is responsible for approximately 1 point in lost stage efficiency for each percentage point in non-dimensional clearance height. This is lower than data in the open literation, which shows values near 2% in efficiency per point in gap height [30] [44], but in accord with the overall focus, this can be regarded as an estimate of the minimum attainable loss under the assumptions made. Appendix B gives a detailed explanation of the tip leakage loss model and a comparison of the results with other models, correlations, and test data.

4.5 Summary of compressor stage performance

Major findings of the compressor stage analysis are as follows.

1. The results of the procedures described in Chapter 3 exhibit similar trends as existing data on axial compressor performance as applied to a "best case," where only unavoidable sources of inefficiency are considered.

2. For representative values of the design parameters for an axial compressor stage, the peak efficiency is approximately 95.5%. With the assumptions made, the peak efficiency occurs at low loading – with values of stage loading coefficient between 0.2 and 0.4. This implies that, from an efficiency standpoint, a large number of lightly loaded stages is preferable to a lighter machine with fewer highly loaded stages. The gradient of efficiency near the maximum value is small, and the stage loading coefficient can be raised from 0.3 to 0.5 at a cost

of one point in stage efficiency.

3. Tip clearance losses are a major factor effecting efficiency for stages near the rear of compressors, where non-dimensional gap heights are large. The current model predicts a drop in efficiency from 95.5% to 93.1% between stages representing the front and rear stages, respectively, of an aero engine high pressure compressor. If the historic clearance derivatives discussed in Appendix B are used, however, there is a much larger difference; the same stages are estimated to have efficiencies of 95% and 87%, respectively.

Chapter 5

Turbine Performance

This chapter presents the findings on turbine stage performance, based on the procedure outlined in Chapter 3. Rational efficiency is used as the performance metric for both uncooled and cooled turbine stages. It is argued that uncooled efficiency should be used as a measure of technology level, and the effect of cooling should be evaluated at the level of the thermodynamic cycle. Uncooled efficiency is thus used as the performance metric, with the effect of cooling flow on stage performance considered in Appendix C. Peak efficiency for an uncooled stage can be calculated by optimizing the stage design variables, given either as blade solidities and inlet swirl angle or Zweifel coefficient and degree of reaction.

5.1 Uncooled stage performance

Results for a baseline turbine stage are given in Figure 5-1. The inputs used are listed in Table 5.1. A peak stage efficiency of 96.5% is observed. The high efficiency is a result of the velocity distribution used, which (1) minimizes overspeeds and (2) keeps the boundary layer shape factor low due to constant surface velocities on both pressure and suction sides. This velocity distribution gives the *lowest possible profile loss under the assumption of turbulent flow.* The blank region represents stages that would require negative suction side velocities with the assumed Zweifel coefficient and velocity distribution. As with the compressor stages considered, the maximum

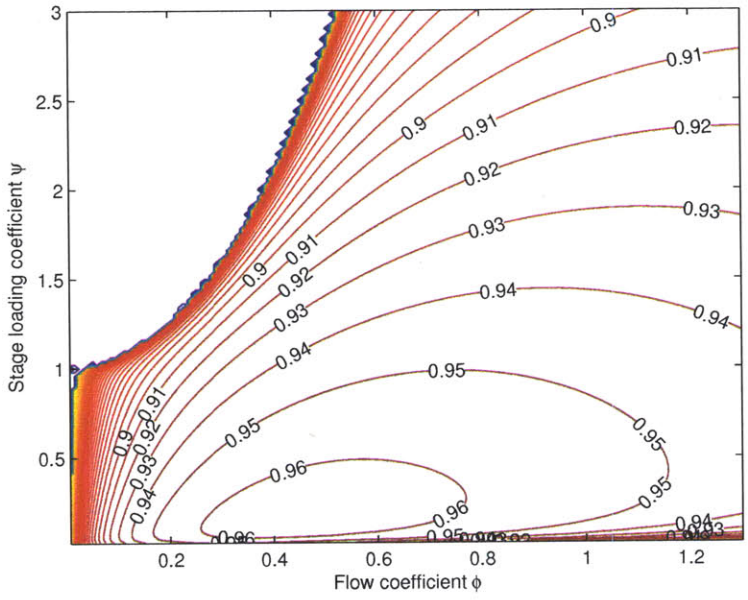


Figure 5-1: Smith chart, baseline uncooled turbine stage

Reynolds number	$\mathrm{Re}_c = V_x c/\nu$	250,000
Aspect ratios	$A_r = h/c$	4
Hub-to-tip ratios	$r_{\mathrm{hub}}/r_{\mathrm{tip}}$	0.75
Gap-to-height ratio	τ/h	0.01
Degree of reaction	Λ	0.5
Zweifel coefficient	Z	1.0

Table 5.1: Inputs for baseline uncooled turbine stage geometry

efficiency occurs at a low value of stage loading coefficient, somewhere between 0.1 and 0.5.

5.2 Optimized stage performance

As with the compressor, the blade spacing and incoming flow angle can be optimized for maximum stage efficiency. Figure 5-2 shows the Smith chart with optimized reaction and Zweifel coefficient (the optimization process leads to some discontinuities in the Smith chart at high loading and low flow coefficient, but near the region of peak efficiency, the results are unaffected by this). Optimization of the turbine stage has a

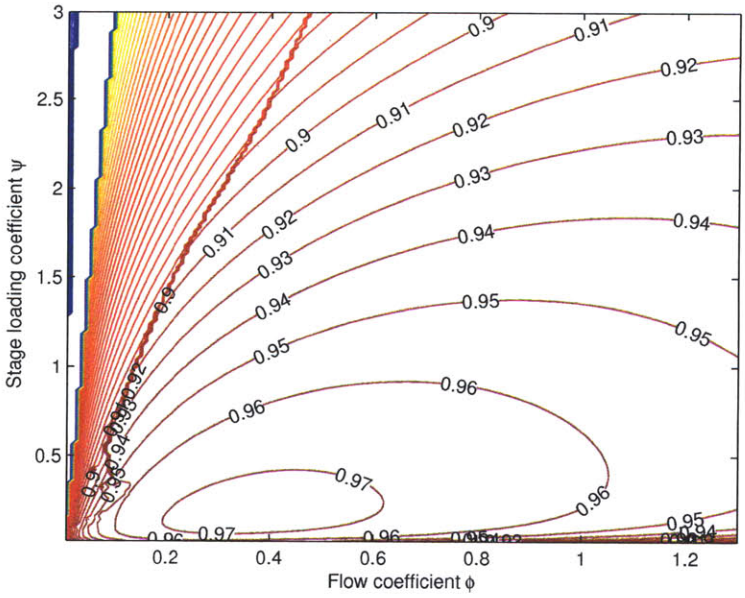


Figure 5-2: Smith chart, optimized baseline uncooled stage

larger effect on peak efficiency than in the compressor, due mainly to the sensitivity of losses to the solidity at different loadings. The maximum efficiency increases to 97.3% as the Zweifel coefficient increases up to values as high as 2.0 at low loadings (below 0.5). As the loading is increased, the Zweifel coefficient drops to keep the suction side velocity down and to keep the pressure side velocity positive, allowing for efficient operation over a greater range of designs than the baseline case.

The degree of reaction decreases to values near zero over the range shown. This behavior is due to the velocity distribution used, which allows the stator to tolerate an increased loading without significant increase in profile losses in order to reduce the loading in the rotor and accompanying tip clearance losses. In practice, the velocity distribution would look very different for a low reaction rotor, and profile losses would become more important. The efficiency is much less sensitive to reaction than blade spacing, however, and high efficiencies can still be attained by optimization of Zweifel coefficient at more realistic values of reaction.

5.3 Comparison to existing data

5.3.1 Dependence on flow and stage loading coefficients

Figure 5-3 shows a turbine Smith chart based on experimental data (Mattingly [31]). Comparison to Figures 5-1 and 5-2 shows agreement in the general trends of efficiency,

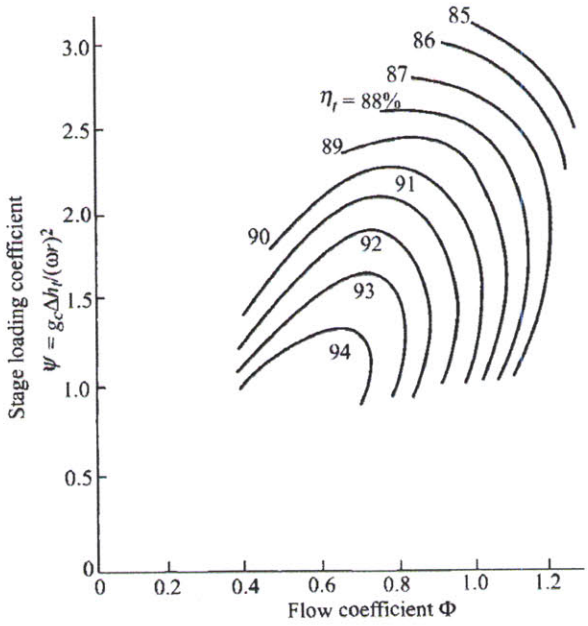


Figure 5-3: Turbine Smith chart based on experimental data, as produced in Mattingly [31]

although the results of the current model have higher efficiency (peak efficiency near 97%, compared to 94%), and the drop in efficiency with changes in stage loading and flow coefficients at the maximum is smaller. This occurs because of the form of the velocity distribution, which minimizes peak velocities so the boundary layer resists separation, even at high loading.

5.3.2 Breakdown of loss sources

Figure 5-4 shows relative magnitudes of the individual loss sources at the location of peak efficiency for the baseline calculation. For the baseline case, the losses in the rotor and stator are approximately equal, and the wake mixing losses are about 13%

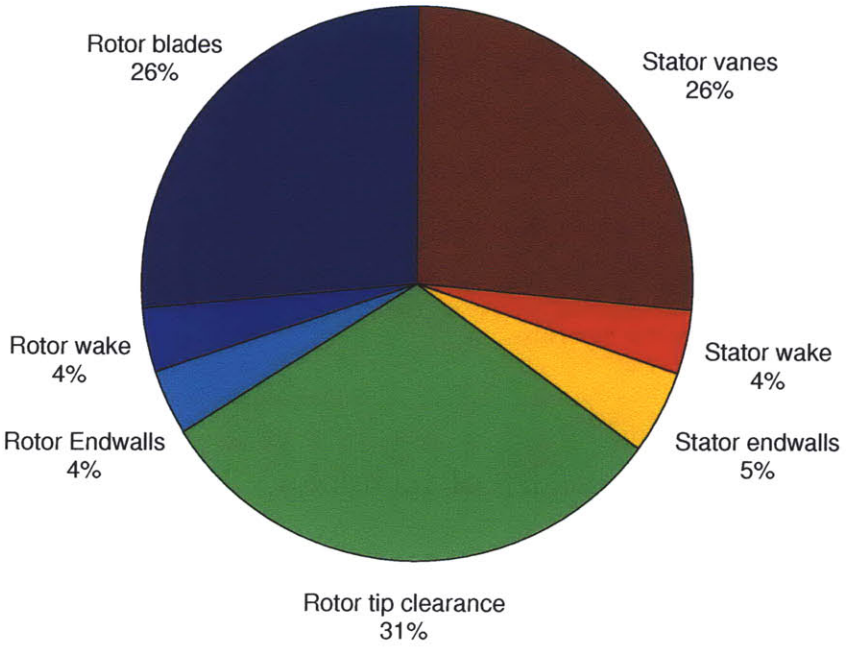


Figure 5-4: Breakdown of losses at peak efficiency for the baseline uncooled turbine stage

of the total profile loss. The rotor tip clearance loss is 31% for a non-dimensional gap height of 0.01, corresponding to a loss of one point in stage efficiency. The profile losses and tip clearance losses dominate because they are approximately proportional to the cube of the suction side velocity.

Optimizing the stage increases the Zweifel coefficient from 1.0 to about 2.0, increasing the endwall area per passage and accompanying losses while increasing the work done per blade. The optimal degree of reaction is well below 50%, unloading the rotor to trade greater stator profile losses for reduced tip clearance losses.

5.4 Turbine efficiency and cooling flows

The drive for higher efficiency and lower weight pushes gas turbine peak cycle temperatures beyond the material capabilities of the turbine, and cooling is needed. The cooling flow can have a large effect on cycle behavior and stage level performance, as seen in Appendix C; losses due to cooling flows can dominate the stage losses. It is argued here, however, that rational efficiency of a cooled stage is not a useful way to characterize stage performance because it includes the effect of losses that are a function of the cycle in which it operates.

5.4.1 Efficiency as a measure of technology level

If the goal of a stage-level efficiency metric is to be a measure of the level of stage design technology, it should be independent of the engine cycle in which the stage operates. The rational efficiency is a function of the mass flow and temperatures ratios of the working fluid flows. These can be different for similarly designed stages operating in different cycles or for different levels of material and cooling technologies. In summary, inclusion of any cooling losses implies a cycle and cooling technology level, and uncooled efficiency is thus the best measure of turbine technology level.

5.4.2 Efficiency as a cycle design parameter

If the efficiency is to serve as an input to cycle calculations, the cooling flow rates and temperatures will not be known a priori. For small cooling mass fractions, the cooling losses will be proportional to the mass flow fraction of the cooling flow. As proposed by Young & Wilcock [49], the mechanical dissipation from mixing of the injected cooling flow can be characterized by a mixing loss coefficient (i.e. a constant multiplied by the cooling flow fraction to obtain the mechanical energy lost), and the entropy generation due to heat transfer across a finite temperature difference can be calculated as a function of the gas temperatures.

5.5 Summary of turbine stage performance

The major findings of the turbine stage analysis are as follows.

1. The results of the loss calculation procedure described in Chapter 3 exhibit similar trends to existing data on axial turbine performance for a "best case" turbine model, where only unavoidable sources of inefficiency are considered.

2. For representative values of the design parameters for an uncooled axial turbine stage, the peak efficiency is approximately 97.3%. This estimate is optimistic due to the assumed blade velocity distribution, which represents an absolute best case with fully turbulent boundary layers.

3. Cooling flow can have a large effect on the rational efficiency of a stage. Since the change in efficiency due to cooling flow is a function of inputs which are tied to the cycle design and material and cooling technologies, uncooled efficiency should be used as a measure of turbine aerodynamic design at the stage level.

Chapter 6

Component Efficiency and Cycle Performance

A main interest is in engine performance, and the benefit of stage efficiency depicted in Chapters 4 and 5 must therefore be evaluated in the context of a thermodynamic cycle. In this chapter, the efficiency of a simple gas turbine cycle (to illustrate some of the overall trends) and of a turbofan engine are evaluated as a function of component efficiency.

6.1 Simple gas turbine

First, a gas turbine generator, consisting of a compressor, burner, and turbine is considered. The turbine powers the compressor and extracts additional power by expanding the flow back to the stagnation temperature entering the compressor. All components are assumed to have the same polytropic efficiency. Cycle temperature ratios are fixed to represent levels of turbine cooling and material technology (see Appendix C for a discussion on turbine cooling and optimal temperature ratios).

If the working fluid is assumed to be a perfect gas with constant specific heat, the thermal efficiency can be expressed as a function of the cycle temperature ratio θ_t,

pressure ratio π_c, and component efficiencies [21]:

$$\eta_{th} = \frac{\left(\alpha - \pi^{\frac{\gamma-1}{\gamma}}\right)\left(1 - \pi^{-\frac{\gamma-1}{\gamma}}\right)}{\beta - \pi^{\frac{\gamma-1}{\gamma}}}, \tag{6.1}$$

where

$$\alpha = \eta_c \eta_t \theta_t, \tag{6.2}$$

$$\beta = 1 + \eta_c(\theta_t - 1). \tag{6.3}$$

Setting the derivative of Equation (6.1) with respect to π_c equal to zero gives the optimal pressure ratio as a function of θ_t and η:

$$\pi^* = \left[\frac{\alpha\beta}{\alpha + \sqrt{\alpha(\beta - \alpha)(\beta - 1)}}\right]^{\frac{\gamma}{\gamma-1}} \tag{6.4}$$

Figure 6-1 shows the maximum thermal efficiency as a function of compressor and turbine polytropic efficiency for $\theta_t = 5.0$, corresponding to turbine entry temperatures

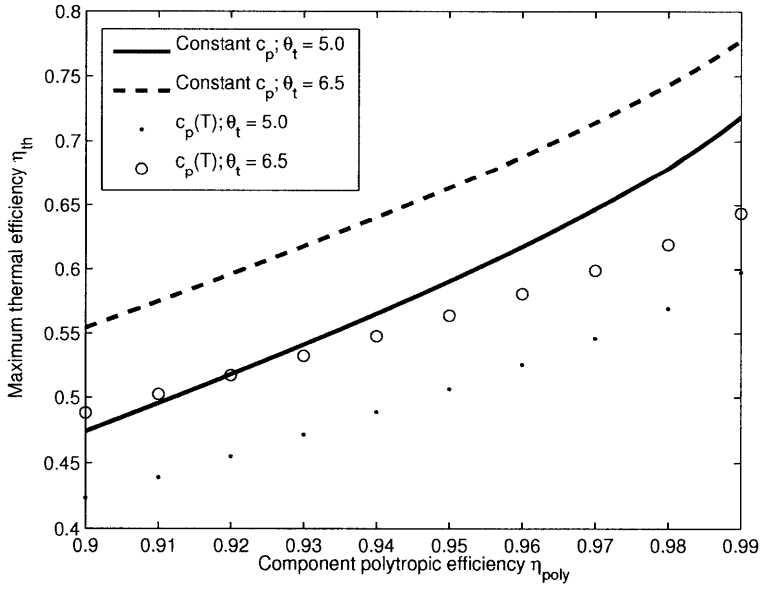


Figure 6-1: Maximum gas turbine thermal efficiency vs component polytropic efficiency

near 1400 K (representing gas turbines for power generation currently in production [32]), and $\theta_t = 6.5$, representing potential increases in turbine entry temperature enabled by improvements in turbine material and cooling technology. To illustrate the effect of temperature-dependent specific heats, values of thermal efficiency for the same cycles, calculated using the model described in Appendix E are also plotted (thermal efficiency is plotted instead of rational efficiency to remain consistent with the constant c_p results). The results show a nearly linear increase in cycle thermal efficiency with component polytropic efficiency. The rate of increase is also diminished with increasing temperature ratio. For $\theta_t = 5.0$, increasing component efficiency from 90% to 95% would increase maximum thermal efficiency from 42% to 51%. For $\theta_t = 6.5$, the same increase in component efficiency results in an increase in maximum thermal efficiency from 49% to 56%.

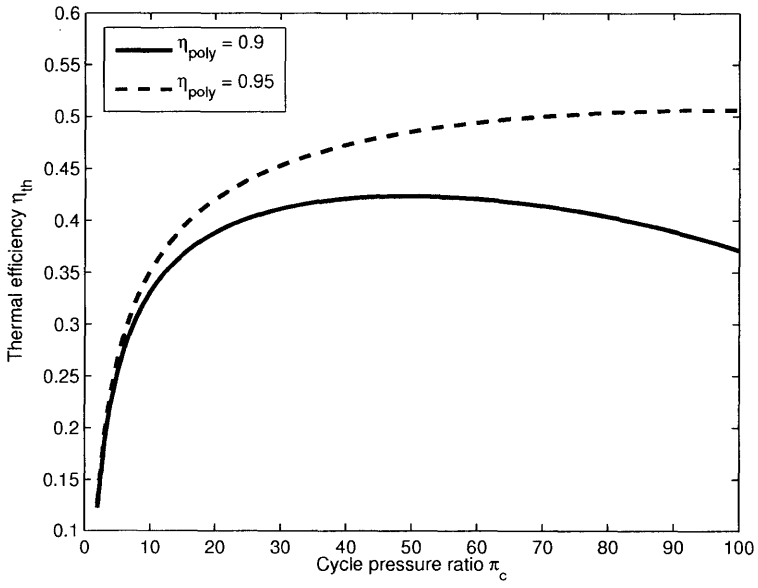


Figure 6-2: Gas turbine thermal efficiency vs cycle pressure ratio, $\theta_t = 5.0$

The importance of optimizing the pressure ratio is illustrated in Figure 6-2, which shows thermal efficiency as a function of cycle pressure ratio for two levels of component efficiency and fixed cycle temperature ratio. If component efficiency is increased while pressure ratio is held fixed, there is a cycle benefit, attributable to the de-

creased amount of irreversibility occurring within the turbomachinery. It is possible, however, to further increase the cycle thermal efficiency by raising the pressure ratio to the new optimum, accounting for an additional 2.14 points in thermal efficiency for the case considered in Figure 6-2. For a best-case scenario, with step changes in both component efficiency *and* turbine material and cooling technologies, the thermal efficiency could be increased from 42% to 56%, corresponding to a 25% decrease in specific fuel consumption.

6.2 Turbofan engine

The turbofan engine is assumed to operate at an altitude of 10 km and a Mach number of 0.8. A cycle temperature ratios of 6.0 is used to represent current combustor exit temperatures [5], and a value of 7.0 is used to represent possible advances in turbine material and cooling technology. The introduction of a fan introduces two additional parameters: fan bypass ratio and fan pressure ratio. As with the simple cycle, the compressor pressure ratio π_c can be optimized as a function of the cycle temperature ratio θ_t and the component polytropic efficiency. Furthermore, for a given bypass ratio, the fan pressure ratio has an optimum value that minimizes the work lost due to inefficiency in the fan the turbine that drives it and the kinetic energy lost in the high speed exiting the core and fan nozzles. Likewise for a given fan pressure ratio, and optimal bypass ratio exists. For the present analysis, a fan pressure ratio of 1.7 is used to represent current fan designs, and a bypass ratio of 20 is used to represent advances enabled by changes in propulsor architecture.

Figure 6-3 shows the engine $TSFC$ as a function of component efficiency for permutations of levels of cooling and fan technologies. Again, minimum fuel consumption decreases almost linearly with increases in component polytropic efficiency. Advances in fan and turbine material and cooling technologies can account for additional increases in performance. The rate of decrease in specific fuel consumption with increase in component polytropic efficiency is greatest for the baseline case, with diminishing returns as other technologies advance.

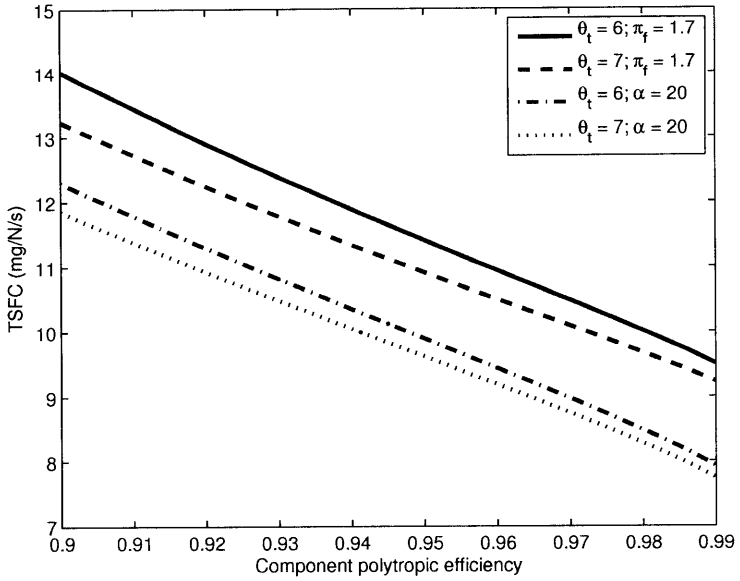


Figure 6-3: Turbofan thrust-specific fuel consumption vs component polytropic efficiency

Table 6.1 shows calculated values of $TSFC$ for some cases of interest. The values of component efficiency used are 90% and 95%, representing something close to values on available commercial turbofan engines and possible future advances given the limits shown in Chapters 4 and 5. For comparison, a CFM56-7 commercial turbofan engine burning jet fuel has a cruise $TSFC$ of 17.06 mg/N/s [16], corresponding to a value of 14.73 mg/N/s for methane (the assumed fuel in the calculations). Achieving the

	η_{poly}	θ_t	Fan tech.	π_c^*	$TSFC$ (mg/N/s)
Baseline	0.9	6	$\pi_f = 1.7$	90.94	14.02
Cooling advances	0.9	6.0	$\pi_f = 1.7$	158.35	13.24 (-5.56%)
Bypass ratio increase	0.9	4.5	$\alpha = 20$	112.32	12.30 (-12.27%)
Component advances	0.95	4.5	$\pi_f = 1.7$	188.14	**11.41 (-18.62%)**
All technologies	0.95	6.0	$\alpha = 20$	491.70	9.62 (-31.38%)

Table 6.1: Changes in engine performance with advances in various technology areas

limits of component efficiency given in Chapters 4 and 5 is seen to provide a greater benefit in fuel consumption than the advances considered in either fan bypass ratio or peak cycle temperatures.

Table 6.1 also shows the optimal pressure ratios for each case, ranging from 90 to almost 500. These values are much higher than current engines (with pressure ratios around 30) due in part to the fact that cooling flows are ignored (see Appendix C for a discussion on the effect of cooling on cycle performance). The trends are still valid, however; advances in component efficiency, turbine entry temperature, and fan bypass ratio will all drive the optimal pressure ratio up. As discussed in Chapter 4 and Appendix B, high efficiency is difficult to maintain at the rear of high pressure compressors. This issue will become increasingly important in the design of the cycle as high pressure ratios and bypass ratios lead to decreased corrected mass flow at the compressor exit.

6.3 Summary of cycle performance

1. For cycle temperature ratios representative of current material and cooling capabilities, an increase in component efficiency from 90% to 95% leads to an increase of approximately 8 points in thermal efficiency, and a reduction of turbofan $TSFC$ by 19%. In comparison, if component efficiency were to stay fixed at 90%, projected advances in cooling and material technologies in the next 30 years [12] would reduce turbofan fuel consumption by 6%, and increasing fan bypass ratios to 20 would reduce $TSFC$ by 12%.

2. Increases in component efficiency, temperature ratio, and bypass ratio drive optimal cycle pressure ratios to levels higher than current machines. A key requirement for realizing such advances is maintaining compressor stage efficiency at the rear of high pressure compressors, where the compressor blades are small, and mechanical details become much more important.

Chapter 7

Conclusion

7.1 Summary

This thesis has examined the limits of turbomachine stage performance and the effect of these limits on overall engine efficiency. The loss metric used at the stage level was a Second Law rational efficiency, which gives a rigorous definition of "ideal" work for all the stage types considered. This metric reduces to the adiabatic and polytropic efficiency for uncooled stages in the incompressible limit. The results presented (Chapters 4 and 5) had agreement with trends seen in current machines, but they indicated an upper limit on stage efficiency four to five points higher than current levels. The effect of these advances on cycle performance was evaluated (Chapter 6). It was seen that small increases in component efficiency can lead to substantial increases in cycle performance if the pressure and temperature ratios are properly selected.

7.2 Conclusions

1. Given the assumptions described, the estimated limits of axial turbomachine stage efficiency are 95.5% for a first high pressure compressor stage and 97.3% for a first low pressure turbine stage.

2. The presence of cooling flows impacts the rational efficiency of cooled turbine stages. However, since the flow rates and temperatures of the various flows entering the stage are a function of the cycle in which they operate as well as the level of material and cooling technology, uncooled efficiency is a more appropriate measure of the level of turbine aerodynamic design technology.

3. The level of compressor and turbine efficiency can have a large impact on overall cycle performance, and advances in turbomachine efficiency leading to appreciable increases in gas turbine cycle thermal efficiency are still to be realized. To fully realize these advances, cycle temperature and pressure ratios should be optimized as a function of component polytropic efficiency, turbine material temperature limits, and blade cooling effectiveness. For temperature ratios and fan pressure ratios representative of current designs, increasing component polytropic efficiency from 90% to 95% leads to a 19% reduction of turbofan cruise thrust-specific fuel consumption.

7.3 Future Work

High efficiency small cores

As discussed in Chapter 6, increased component efficiency leads to an increase in optimal compressor pressure ratio well above values seen in current engines. However, small core size (as is encountered at the back of high pressure ratio compressors) leads to decreases in compressor efficiency. The design of high pressure ratio core compressors with high efficiency thus will be an enabling technology for advanced engines [12]. Examination of the effect of size on compressor polytropic efficiency and of axi-centrifugal configurations is of high interest in this regard.

Profile optimization

Perhaps the crudest approximations made in the current research were the velocity distributions used for blade profiles and the assumption of fully turbulent flow. Rather

than using an assumed velocity profile, a discretized velocity distribution $u(\xi)$ could be considered a design variable which is optimized (constrained by the required blade circulation and Kutta condition) for minimum loss. This could be performed either for a fully turbulent boundary layer, or relaxed to allow regions of laminar flow. Optimizing the velocity profile with transitioning laminar flow would give the best possible performance of a two-dimensional cascade as a function of Reynolds number and transition criteria.

Aircraft-level performance

The current stage-level analysis was performed with design point stage efficiency as the only objective function, and the cycle analysis only attempted to minimize cycle specific fuel consumption. For an aircraft engine, weight and off-design performance must also be considered, with overall mission fuel consumption as the objective function. This means accounting for weight and off-design performance constraints at the stage level. The highest system considered needs to be the aircraft, rather the thermodynamic engine cycle, including mission constraints that drive engine designs towards lower weight with acceptable levels of performance over a range of operating conditions.

Appendix A

Boundary Layer Calculations

The boundary layer calculations used to calculate dissipation on blade surfaces and in trailing wakes is described here. An integral method described by Drela & Giles [11] is used, assuming the flow is incompressible and fully turbulent, and a two-point central finite difference Netwon iteration is used at discreet points along the surface, marching forward to calculate the evolution of the boundary layer given a velocity distribution $u(\xi)$, where u is the streamwise velocity, and ξ is the streamwise arc length coordinate.

A.1 Integral boundary layer formulation

A.1.1 Governing equations

The problem is governed by the integral boundary layer momentum and kinetic energy equations for incompressible flow.

$$\frac{d\theta}{d\xi} + (2+H)\frac{\theta}{u}\frac{du}{d\xi} = \frac{C_f}{2} \tag{A.1}$$

$$\theta\frac{dH^*}{d\xi} + H^*(1-H)\frac{\theta}{u}\frac{du}{d\xi} = 2C_{\mathcal{D}} - H^*\frac{C_f}{2} \tag{A.2}$$

A.1.2 Turbulent Closure

Equations (A.1) and (A.2) are closed by correlations for the skin friction coefficient C_f, kinetic energy shape factor $H^* = \theta^*/\theta$, and dissipation coefficient $C_{\mathcal{D}}$ in terms of the boundary layer momentum thickness θ and shape factor $H = \theta/\delta^*$. The turbulent closure relations described by Drela & Giles [11] are used, assuming incompressible flow.

$$C_f = \frac{0.3e^{-1.33H}}{(\log \mathrm{Re}_\theta)^{1.74+0.31H}} + 0.00011\left[\tanh\left(4 - \frac{H}{0.875}\right) - 1\right] \tag{A.3}$$

$$H^* = \begin{cases} 1.505 + \frac{4}{\mathrm{Re}_\theta} + \left(0.165 - \frac{1.6}{\sqrt{\mathrm{Re}_\theta}}\right)\frac{(H_o - H)^{1.6}}{H}, & H < H_o \\ 1.505 + \frac{4}{\mathrm{Re}_\theta} + (H - H_o)^2\left(\frac{0.04}{H} + \frac{0.007 \ln \mathrm{Re}_\theta}{\left(H - H_o + \frac{4}{\ln \mathrm{Re}_\theta}\right)^2}\right), & H > H_o \end{cases} \tag{A.4}$$

where

$$H_o = \begin{cases} 4, & \mathrm{Re}_\theta < 400 \\ 3 + \frac{400}{\mathrm{Re}_\theta}, & \mathrm{Re}_\theta > 400 \end{cases} \tag{A.5}$$

$$C_{\mathcal{D}} = \frac{H^*}{2}\left[\frac{C_f}{6}\left(\frac{4}{H} - 1\right) + 0.03\left(1 - \frac{1}{H}\right)^3\right] \tag{A.6}$$

A.1.3 Leading edge treatment

The specified velocity profiles have non-zero velocity at the leading edge. In reality, a stagnation point and region of accelerating flow will exist near the trailing edge. This is accounted for by assuming a non-zero boundary layer thickness at the first point in the specified velocity profile, taken to be at some fixed fraction of the chord rather than at the leading edge. Table ?? shows the assumed initial conditions for the calculation. The Reynolds number is meant to represent a critical value, above which the laminar flow near the leading edge starts to transition. The shape factor H is the value for Falkner-Skan similarity profile for the case of zero pressure gradient in the direction of the flow [38]. These assumptions are consistent with results for integral boundary layer calculations for laminar boundary layer growth in regions of acceleration after a leading edge stagnation point.

A.2 Calculation procedure

Equations (A.1) and (A.2) along with Equations (A.3), (A.4), and (A.6) give a system of two equations in terms of two unknowns (H and θ). Equations (A.1) and (A.2) can be rearranged in residual form.

$$\mathcal{R}_1 = \ln\left(\frac{\theta_i}{\theta_{i-1}}\right) - \left(\overline{\frac{C_f\xi}{2\theta}}\right)_i \ln\left(\frac{\xi_i}{\xi_{i-1}}\right) + (\overline{H}_i + 2)\ln\left(\frac{u_i}{u_{i-1}}\right) = 0 \tag{A.7}$$

$$\mathcal{R}_2 = \ln\left(\frac{H_i^*}{H_{i-1}^*}\right) - \left[\left(\overline{\frac{2C_\mathcal{D}\xi}{H^*\theta}}\right)_i - \left(\overline{\frac{C_f\xi}{2\theta}}\right)_i\right] \ln\left(\frac{\xi_i}{\xi_{i-1}}\right) - (\overline{H} - 1)\ln\left(\frac{u_i}{u_{i-1}}\right) = 0 \tag{A.8}$$

where

$$\overline{H}_i = \frac{1}{2}(H_i + H_{i-1}) \tag{A.9}$$

$$\left(\overline{\frac{C_f\xi}{2\theta}}\right)_i = \frac{1}{2}\left(\frac{C_{f,i}\xi_i}{2\theta_i} + \frac{C_{f,i-1}\xi_{i-1}}{2\theta_{i-1}}\right) \tag{A.10}$$

$$\left(\overline{\frac{2C_\mathcal{D}\xi}{H^*\theta}}\right)_i = \frac{1}{2}\left(\frac{2C_{\mathcal{D},i}\xi_i}{H_i^*\theta_i} + \frac{2C_{\mathcal{D},i-1}\xi_{i-1}}{H_{i-1}^*\theta_{i-1}}\right) \tag{A.11}$$

Solution of Equations (A.7) and (A.8) is solved by Newton iteration. If the velocity profile is sufficiently discretized, a good initial guess for H_i and θ_i are the values at the previous station, H_{i-1} and θ_{i-1}. The values are then updated via Newton iteration of the 2×2 system.

$$\begin{bmatrix} \frac{\partial\mathcal{R}_1}{\partial H_i}(H_i^j, \theta_i^j) & \frac{\partial\mathcal{R}_1}{\partial\theta_i}(H_i^j, \theta_i^j) \\ \frac{\partial\mathcal{R}_2}{\partial H_i}(H_i^j, \theta_i^j) & \frac{\partial\mathcal{R}_2}{\partial\theta_i}(H_i^j, \theta_i^j) \end{bmatrix} \begin{bmatrix} \delta H^j \\ \delta\theta^j \end{bmatrix} = \begin{bmatrix} -\mathcal{R}_1(H_i^j, \theta_i^j) \\ -\mathcal{R}_2(H_i^j, \theta_i^j) \end{bmatrix} \tag{A.12}$$

$$H_i^{j+1} = H_i^j + \delta H^j \tag{A.13}$$

$$\theta_i^{j+1} = \theta_i^j + \delta\theta^j \tag{A.14}$$

Appendix B

Tip Clearance Losses

B.1 Clearance loss model

Tip clearance losses are calculated using the simple theory for unshrouded blades presented by Denton [7]. It is assumed the leakage flow through the tip clearance is isentropic, and is driven by the pressure different across the tip. The mechanism of loss is assumed to be the viscous mixing of the injected flow with the main flow on the suction side. Since the leakage flow is small compared to the main flow, it is assumed to mix out to the suction side velocity instantaneously, and the total dissipation over the blade can be calculated as a function of the profile velocity distribution.

$$\frac{\Phi}{\dot{m}V_x^2} = C_D \frac{\tau}{h}\frac{C_s}{c}\sigma \int_0^1 \frac{V_{SS}}{V_x}\left(\frac{V_{SS}}{V_x} - \frac{V_{PS}}{V_x}\right)\sqrt{\left(\frac{V_{SS}}{V_x}\right)^2 - \left(\frac{V_{PS}}{V_x}\right)} d\frac{\xi}{C_s}, \tag{B.1}$$

where C_D is a discharge coefficient; Denton [7], Storer & Cumpsty [41], and Yaras & Sjolander [47] suggest that 0.8 is an appropriate value of C_D. The calculation can be simplified by approximating the pressure difference across the tip as uniform and assuming thin blades with low camber.

$$\frac{V_{SS}}{V_x} - \frac{V_{PS}}{V_x} \approx \frac{\psi}{\sigma\phi} \tag{B.2}$$

$$\frac{V_{SS}}{V_x} + \frac{V_{PS}}{V_x} \approx \frac{2}{\cos\xi} \tag{B.3}$$

Since the loss is nearly proportional to the cube of the suction side velocity, these approximations give the *lowest possible clearance loss under the assumptions* (namely the immediate mixing assumption) by minimizing the magnitude of the assumed V_{SS}.

B.2 Clearance loss magnitudes

Figure B-1 shows calculated loss in efficiency due to rotor tip clearance with non-dimensional gap height of 0.01 for 50% reaction compressor compressor and turbine stages with fixed diffusion factor and Zweifel coefficient, respectively. Inspection

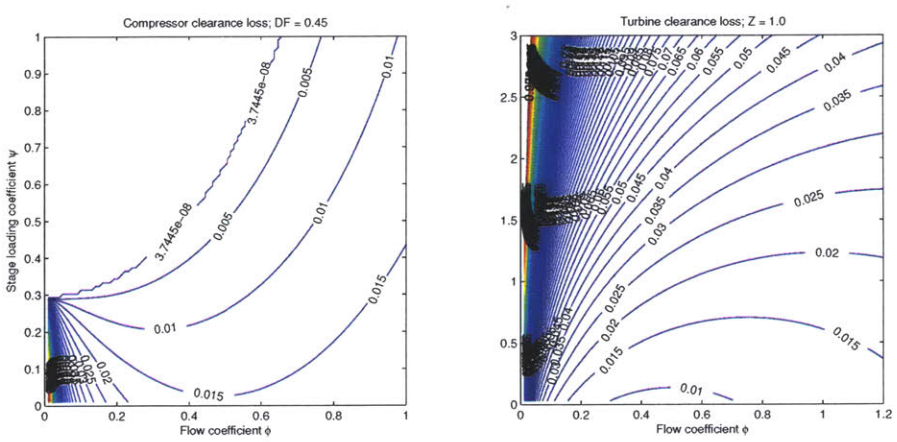


Figure B-1: Loss in efficiency per point in non-dimensional gap height as a function of stage loading and flow coefficients from 50% reaction compressor and turbine stages

of Equation (B.1) shows the clearance loss to be proportional to the gap height, so the losses shown in Figure B-1 can be though of as *clearance derivatives*, the loss in efficiency per point in non-dimensional gap height. For both compressor and turbine, the clearance loss magnitude is seen to depend strongly on blade loading. For compressors, the greater solidity required at higher loadings unloads the rotor, and the loss in efficiency due to tip clearance flow decreases from approximately 1.5% at low loadings to zero at the separation limit. For turbines, the clearance loss increases continually with loading, up to values as high as 5% for reasonable blade loadings.

B.3 Comparison to existing methods and data

Storer & Cumpsty [41] present an approximate prediction method for tip clearance losses using the same mixing analysis as the present method, with the assumption that the flows mix out at the bladerow discharge velocity rather than the suction side velocity. This assumption results in lower predicted losses; for stages comparable to those shown in Figure B-1, the calculated clearance derivatives using their method is less than 0.4. Their method matches experimental data well however, predicting tip clearance losses for a linear cascade [40] to within 10%. The current method overpredicts the loss for the same cascade by 50%. The fact that the model employed Storer & Cumpsty matches experimental data more closely than the current model indicates that the mechanism for loss in tip clearance flows may be more complicated than immediate mixing on the suction side.

Yaras & Sjolander [47] present a similar loss estimation method that assumes the lost work is related to the rate of kinetic energy of the clearance flow *normal to the main flow.* This method also gives lower results than the current model (again by about 50%, but varying with clearance height), but it matches their experimental cascade data [46] well.

Figure B-2 shows a comparison of the calculated clearance derivative of Storer &

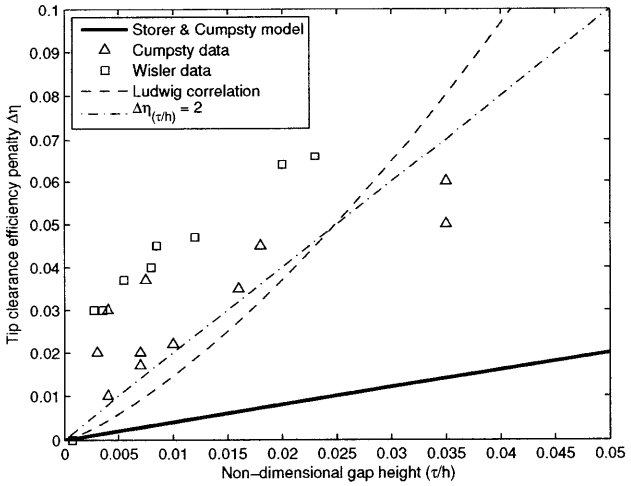


Figure B-2: Comparison of various tip clearance loss measurements and calculations

Cumpsty [41], experimental data for axial turbomachinery presented by Cumpsty [4] and Wisler [44], and a correlation presented by Ludwig [30]. Also shown is a constant-slope line corresponding to a clearance derivative of 2.0.

The method of Storer & Cumpsty (which predicts losses of roughly the same magnitude as the method of Yaras & Sjolander) predicts stage clearance derivatives much lower than those measured in real turbomachines. It is unclear whether this is due to the definition and measurement of clearance losses or if the mechanism of tip clearance loss is different in real stages leading to larger losses than in cascade measurements (Storer & Cumpsty argue the former [41]). Estimates using the present method lie below most of the measured data (on or below the $\Delta\eta_{(\tau/h)} = 2.0$ line for reasonable blade loadings). From these observations is it concluded that the present method provides a reasonable estimate of minimum attainable clearance loss for real turbomachine stages.

Appendix C

Turbine Cooling

The addition of cooling flow has two effects on performance. First, the mixing of the cooling flow with the main flow generates additional entropy via heat transfer across a finite temperature difference. Second, the cycle is fundamentally changed: the turbine inlet temperature rises, and the required cooling flow decreases the temperature of the main flow as the two are mixed within the cooled portion of the turbine. The impact of these effects on both stage and cycle efficiency is considered here.

C.1 Stage performance

This additional entropy generation and the presence of an injected cooled flow in a cooled turbine stage can have a significant effect on the rational efficiency. It was argued in Chapter 5 that for purposes of measuring technology level or incorporation into cycle calculations, uncooled efficiency is the best metric for turbine stage efficiency. Young & Horlock [48] propose, however, that rational efficiency be used to characterize turbine efficiency, as it is the cooled efficiency definition with the "soundest thermodynamic foundation."

C.1.1 Rational efficiency definition

Two flows enter a cooled turbine stage at different states and exit at a mixed out state after having produced some work. The overall change in exergy is defined using the mass-weighted average of the exergy of the two incoming flows. Figure C-1 gives a pictorial representation of the flow of exergy through a generic work-producing component with two incoming fluid flows. Despite the presence of multiple incoming

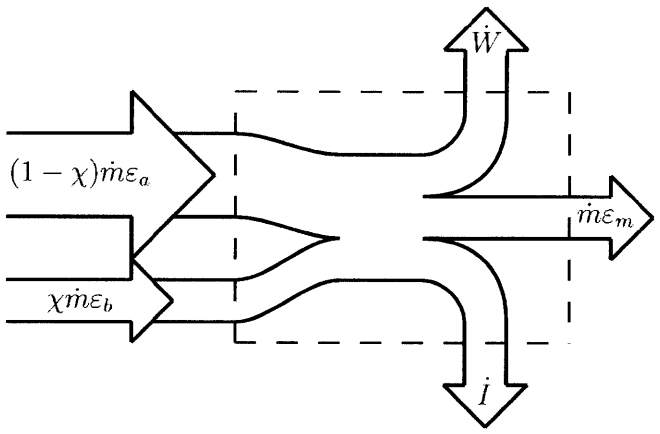


Figure C-1: Exergy flow diagram for component with multiple incoming flows (a and b) producing work ($\dot{W}$) irreversibly ($\dot{I}$) and mixing (to state m)

flows, the exergetic effectiveness is still precisely expressed as the ratio of the useful work to the decrease in mass-averaged flow exergy.

$$\epsilon_t = \frac{(1-\chi)(h_{t1}-h_{t2})+\chi(h_{t\text{cool}}-h_{t2})}{(1-\chi)(h_{t1}-T_0 s_1)+\chi(h_{t\text{cool}}-T_0 s_{\text{cool}})-(h_{t2}-T_0 s_2)}. \tag{C.1}$$

There is no simple conversion back to adiabatic or polytropic efficiency as there was for the effectiveness of a single-stream (uncooled) component.

C.1.2 Thermal mixing loss

If the cooling mass flow is small relative to the main flow, the lost work due to entropy generation is equal to the work of a reversible Carnot engine operating between the

temperatures of the two flows [13] [28] [50].

$$\frac{T_{t2}ds_Q}{c_p} = \frac{\chi}{1-\chi}\int_{T_{t2}}^{T_{t,inj}}\left(1-\frac{T_{t2}}{T}\right)dT = \frac{\chi}{1-\chi}\left[(T_{t,\text{inj}}-T_{t2}) - T_{t2}\ln\left(\frac{T_{t,\text{inj}}}{T_{t2}}\right)\right] \tag{C.2}$$

Effect of compressibility

Examination of Equations (2.22), (2.24), and (2.25) shows the mechanical dissipation can be normalized by a kinetic energy flux term $\dot{m}V_{\text{ref}}^2$, where V_{ref} is a reference velocity. This normalization allows for comparison to the work of a turbomachine stage by relating the work to the reference velocity using the stage geometry and the flow coefficient and stage loading coefficient. The decrease in stage efficiency is finite the incompressible limit, even though the stage work approaches zero.

The thermal mixing loss, however, is normalized in Equation (C.2) by the gas specific heat c_p, and expressed in terms of only mass fractions and stagnation temperatures. When divided by a stage work term, the thermal mixing efficiency debit has a $1/M^2$ dependence, because the entropy generated in the thermal mixing process is independent of Mach number, while the stage work is proportional to M^2. The result is a singularity in the inefficiency as Mach number approaches zero.

A way to evaluate the effect of heat transfer in the mixing of two streams on cooled turbine stage efficiency is to use a representative Mach number to compare the entropy generation to the stage work. A rotor inlet Mach number of unity is generally used in cooled turbine stage calculations, representing a choked nozzle guide vane upstream.

C.1.3 Rational efficiency of a cooled stage

The rational stage efficiency of a cooled turbine is plotted in Figure C-2. The stage design parameters are described in Table C.1 and represent the first stage of the turbine of a modern commercial turbofan engine [16]. The peak efficiency is 94.9%, a substantial drop from the values above 97% seen in Figure 5-2. Most of the increased loss is due to the cooling flow, with some attributed to the lower aspect ratio and larger tip clearance. The general trends in efficiency remain unchanged, however, the

unseparated regime is slightly decreased from the optimized uncooled case due to the presence of additional loss sources.

The breakdown of losses at the location of peak efficiency is shown in Figure C-3. The cooling loss dominates, accounting for over half the losses in the stage. The mechanical mixing loss is the largest component of the entropy generation attributable to the cooling flow; the thermal mixing only accounts for 17% of the rotor cooling loss and 25% of the stator cooling loss.

Reynolds number	$\mathrm{Re}_c = V_x c/\nu$	300,000
Aspect ratios	$A_r = h/c$	1.5
Hub-to-tip ratios	$r_{\mathrm{hub}}/r_{\mathrm{tip}}$	0.85
Gap-to-height ratio	τ/h	0.02
Rotor cooling flow fraction	$\chi_r = \dot{m}_{\mathrm{cool},r}/\dot{m}$	0.02808
Stator cooling flow fraction	$\chi_s = \dot{m}_{\mathrm{cool},s}/\dot{m}$	0.01931
Cooling flow temperature ratio	T_{tc}/T_{t1}	0.5681
Inlet Mach number	M_1	1

Table C.1: Cooling input parameters for baseline cooled turbine stage

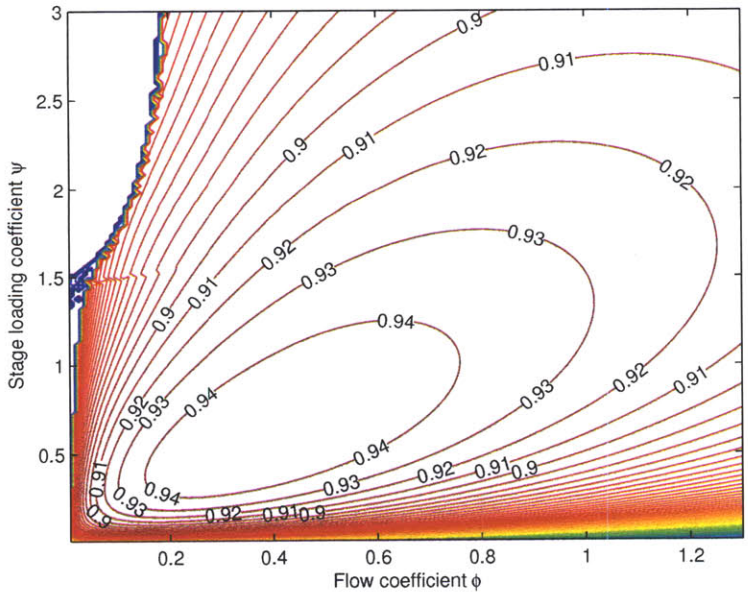


Figure C-2: Smith chart, optimized cooled turbine stage

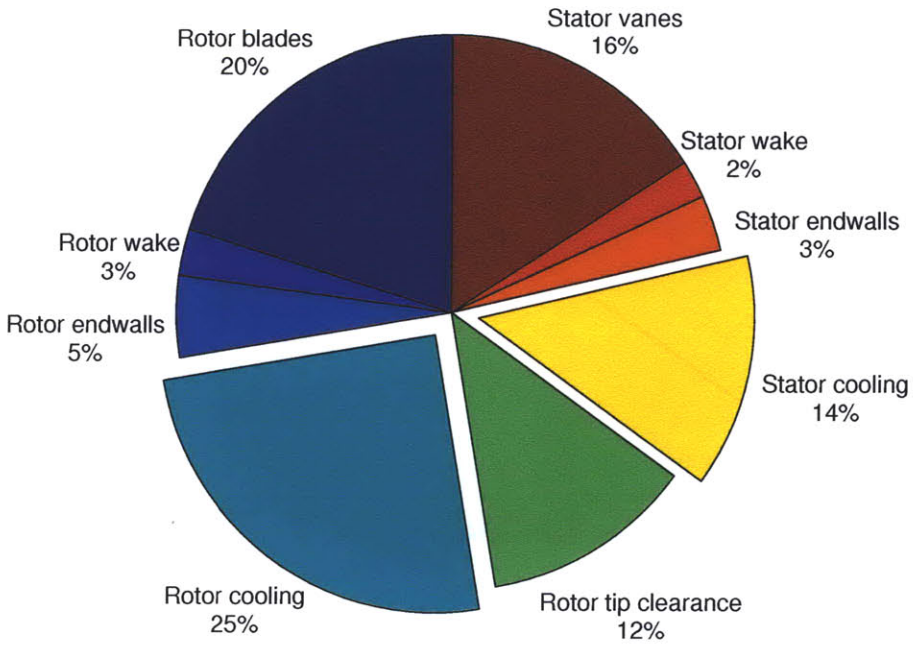


Figure C-3: Breakdown of losses at peak efficiency for the optimized baseline cooled turbine stage

C.2 Cycle implications

As the total required cooling flow fraction increases, the cooling losses increases, as does the lost opportunity for work due to injecting cooling flow after the first turbine rotor. Wilcock, Young, & Horlock [43] show that an optimal combustor exit temperature below the stoichiometric limit exists for a given level of turbomachine efficiency and turbine material and cooling technology. Furthermore, numerical experiments by Horlock, Watson, & Jones [22] suggest the effect of turbine cooling on cycle performance is adequately captured by assuming all the cooling flow is injected upstream of the first turbine rotor.

Figure C-4 shows optimal temperature ratios as a function of allowable metal temperature for a gas turbine generator (pressure ratio has also been optimized at

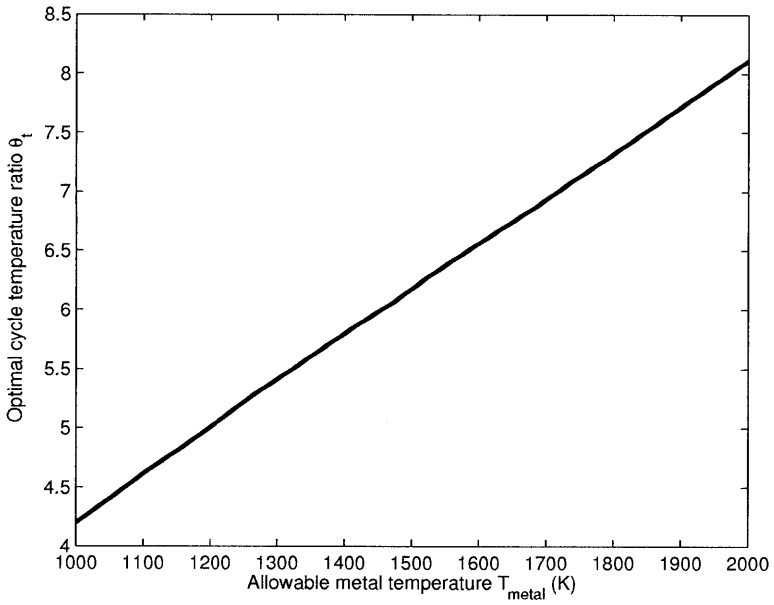


Figure C-4: Optimal gas turbine temperature ratio as a function of allowable turbine metal temperature

each point), obtained using the perfect gas cycle model described in Appendix E. The required cooling rates are calculated using the procedure of Horlock, Watson, & Jones [22] with component efficiency and cooling technology characterized by the parameters listed in Table C.2 (note: the optimum cycle temperature ratio is most sensitive to allowable metal temperature, and fairly insensitive to component efficiency and the level of cooling technology).

Component efficiency	η_{poly}	0.9
Film cooling effectiveness	$\varepsilon_{\text{film}}$	0.3
Weighted Stanton number	St_A	0.09

Table C.2: Component and cooling technology levels for optimum cycle temperature ratio calculation

Denton [7] and Horlock [21] argue that the thermal efficiency of a cooled gas turbine cycle is approximately equal to that of the same cycle without any cooling flow. This assumption is used in Chapter 6, where values of cycle temperature ratio θ_t are fixed to represent levels of turbine material technology. In this way, uncooled stage

efficiency, as calculated in Chapter 5, can be used as the cycle input characterizing turbine performance.

Appendix D

Turbomachine stage performance calculation procedure

The loss in stage efficiency is estimated by calculating the entropy generated by each of the loss mechanisms listed in section 3.3, summing them, and dividing by the work input of the stage:

$$\eta_{\text{stage}}^{\pm 1} = 1 - \sum \Delta\eta = 1 - \sum \frac{T\Delta s}{\Delta h} = 1 - \sum \frac{\Phi}{\dot{m}\Delta h} - \sum \frac{T\Delta s_Q}{\Delta h} \tag{D.1}$$

It will be seen that the efficiency can be calculated as a function of a small number of stage parameters, some of which are considered independent, some of which can be fixed given the location or type of stage being considered (design parameters), and the rest of which can be optimized (design variables) given fixed values of the rest.

D.1 Flow angles

Assuming a repeating stage ($\alpha_3 = \alpha_1$) and constant radius, all the flow angles can be calculated in terms of either a specified inter-stage swirl α_1 or degree of reaction Λ, the *flow coefficient* $\phi = V_x/U$, and the *stage loading coefficient* $\psi = \Delta h_t/U^2$ using trigonometric relations and the Euler turbine equation.

Compressor

$$\alpha_1 = \begin{cases} \alpha_{1,\text{spec}} \\ \tan^{-1}\left(\dfrac{2(1-\Lambda_{\text{spec}})-\psi}{2\phi}\right) \end{cases} \tag{D.2}$$

$$\alpha_2 = \tan^{-1}\left(\frac{\psi}{\phi} + \tan\alpha_1\right) \tag{D.3}$$

$$\alpha_3 = \alpha_1 \tag{D.4}$$

$$\beta_1 = \tan^{-1}\left(\frac{1}{\phi} - \tan\alpha_1\right) \tag{D.5}$$

$$\beta_2 = \tan^{-1}\left(\frac{1}{\phi} - \tan\alpha_2\right) \tag{D.6}$$

Turbine

$$\alpha_1 = \begin{cases} \alpha_{1,\text{spec}} \\ \tan^{-1}\left(\dfrac{2(1-\Lambda_{\text{spec}})+\psi}{2\phi}\right) \end{cases} \tag{D.7}$$

$$\alpha_2 = \tan^{-1}\left(\frac{\psi}{\phi} - \tan\alpha_1\right) \tag{D.8}$$

$$\alpha_3 = \alpha_1 \tag{D.9}$$

$$\beta_1 = \tan^{-1}\left(\tan\alpha_1 - \frac{1}{\phi}\right) \tag{D.10}$$

$$\beta_2 = \tan^{-1}\left(\tan\alpha_2 + \frac{1}{\phi}\right) \tag{D.11}$$

D.2 Camber lengths

The meridional blade surface length C_s will be an important variable in calculating the blade surface dissipation. The blades are assumed to be thin, so the camber length, which can be calculated given a camber shape, is a suitable approximation for the surface length.

Compressor

Compressor airfoils are assumed to have circular arc camber lines, so the surface length relative to the chord can be calculated as

$$\left(\frac{C_s}{c}\right)_c = \frac{\alpha_{\text{in}} - \xi_c}{\sin(\alpha_{\text{in}} - \xi_c)}, \tag{D.12}$$

where ξ is the stagger angle,

$$\xi_c = \frac{1}{2}(\alpha_{\text{in}} + \alpha_{\text{out}}). \tag{D.13}$$

Turbine

Turbine airfoils are assumed to have parabolic camber lines, so the surface length relative to the chord can be calculated as

$$\left(\frac{C_s}{c}\right)_t = \cos\xi_t \left[\frac{(B+2A)\sqrt{A+B+C} - B\sqrt{C}}{4A} + \frac{4AC - B^2}{8A^{1.5}} \ln\left(\frac{2A+B+2\sqrt{A(A+B+C)}}{B+2\sqrt{AC}}\right)\right], \tag{D.14}$$

where ξ is the stagger angle,

$$\xi_t = \tan^{-1}\left(\frac{1}{2}(\tan\alpha_{\text{out}} - \tan\alpha_{\text{in}})\right), \tag{D.15}$$

and

$$A = 4\left[\frac{1}{2}(\tan\alpha_{\text{in}} + \tan\alpha_{\text{out}})\right]^2 \tag{D.16}$$

$$B = 4\left[\frac{1}{2}(\tan\alpha_{\text{in}} + \tan\alpha_{\text{out}})\right][-\tan\alpha_{\text{in}}] \tag{D.17}$$

$$C = 1 + \tan^2\alpha_{\text{in}} \tag{D.18}$$

D.2.1 Blade spacing

A blade row's solidity may be specified or calculated in terms of the diffusion factor for a compressor row or Zweifel coefficient for a rotor row.

Diffusion factor

The diffusion factor is a measure of the amount of diffusion that occurs in a compressor cascade, which has historically been used to empirically predict profile loss coefficients for compressor stages [25]. For incompressible flow, it is expressed as

$$DF = 1 - \frac{\cos \alpha_{\text{in}}}{\cos \alpha_{\text{out}}} + \frac{\cos \alpha_{\text{in}}(\tan \alpha_{\text{in}} - \tan \alpha_{\text{out}})}{2\sigma_c}. \tag{D.19}$$

Rearranging, the solidity can be calculated in terms of a specified diffusion factor.

$$\sigma_c = \frac{\cos \alpha_{\text{in}}}{2\left(DF - 1 + \frac{\cos \alpha_{\text{in}}}{\cos \alpha_{\text{out}}}\right)} \frac{\psi}{\phi} \tag{D.20}$$

Zweifel coefficient

The Zweifel coefficient is a measure of turbine blade loading, comparing the tangential force on a blade to the force if the entire pressure side surface was at the inlet stagnation pressure and the suction side surface was at the exit static pressure [6]. For incompressible flow, it can be expressed as

$$Z = 2\cos^2 \alpha_{\text{out}}(\tan \alpha_{\text{in}} + \tan \alpha_{\text{out}})\frac{s}{c_x}. \tag{D.21}$$

Rearranging, the solidity can be calculated in terms of a specified Z.

$$\sigma_t = \frac{2\cos^2 \alpha_{\text{out}}}{Z \cos \xi_t} \frac{\psi}{\phi} \tag{D.22}$$

D.3 Velocity distribution

In order to calculate the dissipation on various solid surfaces and in mixing of various nonuniform flows, the assumed velocity profiles described in section 3.2 are used to calculate flow velocities.

Compressor blade profile

The compressor blading is assumed to have linear velocity distributions of the form

$$V(s) = \left(1 - \frac{s}{C_s}\right)(V_{\text{in}} \pm \Delta V) + \frac{s}{C_s} V_{\text{out}}, \tag{D.23}$$

where s is the distance along the blade surface. The inlet an exit velocities are related through continuity for an incompressible blade row passage.

$$V_x = V_{\text{in}} \cos \alpha_{\text{in}} = V_{\text{out}} \cos \alpha_{\text{out}} \tag{D.24}$$

The leading edge velocity jump ΔV is calculated by matching the circulation around a blade to the correct amount of turning through the blade passage.

$$\Delta V = \frac{V_x}{\sigma(C_s/c)} \frac{\psi}{\phi} \tag{D.25}$$

Combining Equations (D.23)-(D.25), the pressure side (PS) and suction side (SS) velocity distributions can be written as follows, normalized by the reference velocity (taken to be the inlet velocity, in keeping with conventional compressor stage analysis).

$$\frac{V_{PS}(s)}{V_{\text{in}}} = \left(1 - \frac{s}{C_s}\right)\left(1 - \frac{\cos \alpha_{\text{in}}}{\sigma(C_s/c)} \frac{\psi}{\phi}\right) + \frac{s}{C_s} \frac{\cos \alpha_{\text{in}}}{\cos \alpha_{\text{out}}} \tag{D.26}$$

$$\frac{V_{SS}(s)}{V_{\text{in}}} = \left(1 - \frac{s}{C_s}\right)\left(1 + \frac{\cos \alpha_{\text{in}}}{\sigma(C_s/c)} \frac{\psi}{\phi}\right) + \frac{s}{C_s} \frac{\cos \alpha_{\text{in}}}{\cos \alpha_{\text{out}}} \tag{D.27}$$

For the endwall loss calculation, the velocity will be desired as a function of the *axial* distance x through the blade row. The transformation from s to x can be made

using the assumption that the blade surface is a circular arc.

$$\frac{s}{C_s} = \left(\frac{R}{c}\right)\left(\frac{C_s}{c}\right)^{-1}\left[\alpha_{\text{in}} - \sin^{-1}\left(\sin\alpha_{\text{in}} - \frac{x}{c_x}\frac{c}{R}\frac{c_x}{c}\right)\right], \tag{D.28}$$

where

$$\left(\frac{R}{c}\right) = \frac{1}{2\sin\left(\frac{\alpha_{\text{in}}-\alpha_{\text{out}}}{2}\right)} \tag{D.29}$$

$$\left(\frac{c_x}{c}\right) = \cos\xi \tag{D.30}$$

D.3.1 Turbine blade profile

The turbine blade velocity profile is rectangular, with constant velocities on the pressure and suction surfaces, defined in terms of an average velocity $\overline{V}$ and a difference term ΔV:

$$V = \overline{V} \pm \Delta V. \tag{D.31}$$

The velocity difference ΔV is calculated using Stokes' theorem, setting the circulation around the contour of a single passage *outside* the blade boundary layers to zero.

$$\Delta V = \frac{V_x}{2\sigma(C_s/c)}\frac{\psi}{\phi} \tag{D.32}$$

The average velocity is calculated by equating the integral of the pressure difference across the blade (calculated using Bernoulli's equation) to the change in angular momentum of the flow through the passage.

$$\overline{V} = \left(\frac{C_s}{c}\right)\frac{V_x}{\cos\xi_t} \tag{D.33}$$

Combining Equations (D.31)-(D.33) and (D.24), the turbine blade velocities can be written as follows, normalized by the passage exit velocity.

$$\frac{V_{PS}}{V_{\text{out}}} = \left(\frac{C_s}{c}\right)\frac{\cos\alpha_{\text{out}}}{\cos\xi_t} - \frac{\cos\alpha_{\text{out}}}{2\sigma(C_s/c)}\frac{\psi}{\phi} \tag{D.34}$$

$$\frac{V_{SS}}{V_{\text{out}}} = \left(\frac{C_s}{c}\right)\frac{\cos\alpha_{\text{out}}}{\cos\xi_t} + \frac{\cos\alpha_{\text{out}}}{2\sigma(C_s/c)}\frac{\psi}{\phi} \tag{D.35}$$

Endwalls

The endwall velocity is assumed to vary linearly from blade to blade in the reference frame of the blades.

$$\frac{V_{\text{wall}}(x,y)}{V_{\text{ref}}} = \frac{V_{PS}(x)}{V_{\text{ref}}} + \frac{y}{W}\left(\frac{V_{SS}(x)}{V_{\text{ref}}} - \frac{V_{PS}(x)}{V_{\text{ref}}}\right), \tag{D.36}$$

where W is the blade pitch, and V_{PS} and V_{SS} are given by Equations (??) and (??) for a compressor stage and Equations (D.34) and (D.35) for a turbine stage.

The hub is assumed to be locked to the frame of the blade, but the outer casing of rotor rows is assumed to move relative to the blades. A correction is made by calculating a relative stagger angle, which is the angle between the axial velocity V_x and the vector sum of the blade-relative velocity and the rotational velocity of the tip of the blade $U_{\text{tip}} = \omega r_{\text{tip}}$.

$$\xi_{\text{rel}} = \tan^{-1}\left(\frac{2}{\phi(1+(r_{\text{hub}}/r_{\text{tip}}))} - \tan\xi\right), \tag{D.37}$$

which can be used to approximate the velocity of the flow through a rotor passage relative to the stationary casing.

$$\frac{V_{\text{wall,rel}}}{V_{\text{ref}}} = \frac{V_{\text{wall}}}{V_{\text{ref}}}\frac{\cos\xi}{\cos\xi_{\text{rel}}} \tag{D.38}$$

D.4 Losses

Blade boundary layer dissipation

The integral boundary layer calculations described in Appendix A is used to evaluate the boundary layer properties at the trailing edges of the rotor blade and stator vane profiles for the stage, given the blade profile velocity distribution described by Equations (D.23) and (D.31) and a supplied Reynolds number. The dissipation on each blade surface can be calculated using Equation (2.22), and the deficit in efficiency due to dissipation in the boundary layer can be calculated by dividing by the stage work.

$$\Delta\eta_{\text{surf}} = \frac{\Phi_{\text{surf}}}{\dot{m}\Delta h_t} = \frac{1}{2}\sigma\left(\frac{C_s}{c}\right)\left(\frac{1}{\cos\alpha_{\text{out}}}\right)^3 \frac{\theta^*_{TE}}{C_s}\frac{\phi^2}{\psi} \tag{D.39}$$

Wake mixing dissipation

The dissipation that occurs as the viscous wakes mix out downstream of the bladerows is described by Equation (2.24). The efficiency deficit due to the mixing out of the wakes[1] can be calculated from the boundary layer properties at the trailing edge of each bladerow and the stage work.

$$D = \left(\frac{\delta^*_{\text{TE}}}{C_s}\right)\left(\frac{C_s}{c}\right)\frac{\sigma}{\cos\alpha_{\text{out}}} \tag{D.40}$$

$$M = \left(\frac{\theta_{\text{TE}}}{C_s}\right)\left(\frac{C_s}{c}\right)\frac{\sigma}{\cos\alpha_{\text{out}}} \tag{D.41}$$

$$K = \left(\frac{\theta^*_{\text{TE}}}{C_s}\right)\left(\frac{C_s}{c}\right)\frac{\sigma}{\cos\alpha_{\text{out}}} \tag{D.42}$$

$$\alpha_m = \tan^{-1}\left[\tan\alpha_{\text{out}}\frac{1-D-M}{(1-D)^2}\right] \tag{D.43}$$

[1]It should be noted that the unsteadiness as a wake travels though a downstream bladerow can lead to a recovery of some of the energy that would be lost in the wake were the bladerow isolated [39], thus Equation (D.44) is an *overestimate* of the loss in efficiency due to wake mixing.

$$\begin{aligned}\Delta\eta_{\text{wake}} =& \frac{\Phi_{\text{wake}}}{\dot{m}\Delta h_t} \\ =& \frac{\phi^2}{\psi}\left\{[M-(1-D)+(1-D)^2](1-D)+\frac{1}{2}\left[\frac{(1-D)-K}{\cos^2\alpha_{\text{out}}}-\frac{(1-D)^3}{\cos^2\alpha_m}\right]\right\}\end{aligned} \tag{D.44}$$

Endwall boundary layer dissipation

The endwall losses are calculated using the constant $C_{\mathcal{D}}$ approximation (Equation (2.23), $C_{\mathcal{D}} = 0.002$) and the endwall velocity distribution described in sections 3.2 and D.3. Again the deficit in efficiency can be calculated by dividing the dissipation by the stage work.

$$\Delta\eta_{\text{wall}} = \frac{\Phi_{\text{wall}}}{\dot{m}\Delta h_t} = C_{\mathcal{D}}\frac{\phi^2}{\psi}\left(\frac{W(r_{\text{wall}})}{W_{ML}}\right)\frac{1}{A_r}\cos\xi\int_0^1\int_0^1\left(\frac{u}{V_x}\right)^3 d(x/c_x)d(y/W(r)), \tag{D.45}$$

where $W(r)$ is the blade pitch at radius r_{wall}, and W_{ML} is the mean line blade pitch. The pitch at the hub and the casing can be calculated in terms of the hub-to-tip ratio of the stage.

$$\frac{W(r_{\text{hub}})}{W_{ML}} = \frac{2}{1+(r_{\text{hub}}/r_{\text{tip}})^{-1}} \tag{D.46}$$

$$\frac{W(r_{\text{tip}})}{W_{ML}} = \frac{2}{1+(r_{\text{hub}}/r_{\text{tip}})} \tag{D.47}$$

The form of the compressor endwall velocity is not amenable to integration, so a 5×5 Gaussian quadrature is used to approximate the integral.

$$\Delta\eta_{c,\text{wall}} = C_{\mathcal{D}}\frac{\phi^2}{\psi}\frac{\cos\xi_c}{A_r\cos^3\alpha_{\text{in}}}\left(\frac{W(r_{\text{wall}})}{W_{ML}}\right)\frac{1}{4}\sum_j\sum_i w_i w_j\left(\frac{V_{\text{wall}}(x_i,y_j)}{V_{\text{in}}}\right)^3, \tag{D.48}$$

where w_i and w_j are the Gaussian quadrature weights, and x_i and x_j are the corresponding evaluation coordinates.

The simple form of the turbine velocity distribution leads to an analytical solution

to the integral.

$$\Delta\eta_{t,\text{wall}} = C_{\mathcal{D}}\frac{\phi^2}{\psi}\frac{\cos\xi_t}{A_r\cos^3\alpha_{\text{out}}}\left(\frac{W(r_{\text{wall}})}{W_{ML}}\right)\frac{V_{PS}^3 + V_{PS}^2\Delta V + \frac{4}{3}V_{PS}\Delta V^2 + 2\Delta V^3}{V_{\text{out}}^3} \tag{D.49}$$

Tip clearance flow dissipation

Tip clearance losses are modeled using the model of Denton [7], described in detail in Appendix B. The mechanism of loss is the mixing of the clearance flow with the flow on the suction side of the blade tip, and the dissipation is given in Equation (B.1). The deficit in efficiency can be calculated by dividing the dissipation by the total stage work.

$$\Delta\eta_{\text{gap}} = \frac{\Phi_{\text{gap}}}{\dot{m}V_x^2}\frac{\phi^2}{\psi} = C_D\frac{\tau}{h}\frac{C_s}{c}\frac{\phi^2}{\psi}\sigma\int_0^1\frac{V_{SS}}{V_x}\left(\frac{V_{SS}}{V_x} - \frac{V_{PS}}{V_x}\right)\sqrt{\left(\frac{V_{SS}}{V_x}\right)^2 - \left(\frac{V_{PS}}{V_x}\right)}d\frac{\xi}{C_s}, \tag{D.50}$$

where

$$\frac{V_{SS}}{V_x} - \frac{V_{PS}}{V_x} \approx \frac{\psi}{\sigma\phi}, \tag{D.51}$$

$$\frac{V_{SS}}{V_x} + \frac{V_{PS}}{V_x} \approx \frac{2}{\cos\xi}. \tag{D.52}$$

Cooling flow losses

For cooled turbine stages, the cooling flow loss is evaluated using the two-dimensional mixing control volume described in section 2.3.3. The thermal mixing losses need to be calculated, and the stagnation temperatures are characterized by a cooling temperature ratio T_{tc}/T_{t1}. Equation (C.2) can be expressed as an efficiency debit term when divided by the $\Delta h_t/c_p$; for a perfect gas, this is equal to the drop in stagnation across the rotor if no cooling flow is present. A temperature drop term $\Delta T_t/T_{t1}$ is calculated in terms of the loading and flow coefficients, an effective Mach number (set to unity to represent choked flow exiting a nozzle upstream), and an

assumed ratio of specific heats γ.

$$\frac{\Delta T_t}{T_{t1}} = (\gamma - 1)\frac{\psi}{\phi^2}\frac{\cos\alpha_1 M_1}{1 + \frac{\gamma-1}{2}M_1^2} \tag{D.53}$$

Once the rotor work is established, the ratio of stagnation temperature to inlet stagnation temperature can be calculated downstream of both rows, taking into account the cooling flows injected into each.

$$\frac{T_{t2}}{T_{t1}} = \frac{1 - \chi_r - \chi_s}{1 - \chi_s}\left(1 - \frac{\Delta T_t}{T_{t1}}\right) + \frac{\chi_r}{1 - \chi_s}\frac{T_{tc}}{T_{t1}} \tag{D.54}$$

$$\frac{T_{t3}}{T_{t2}} = (1 - \chi_s)\frac{T_{t2}}{T_{t1}} + \chi_s\frac{T_{tc}}{T_{t1}} \tag{D.55}$$

These temperature ratios with the assumed mass flow ratios are enough to calculate the loss in efficiency, using Equations (2.25) and (C.2). A cooling flow mixing angle of $\zeta_{\text{cool}} = 40°$ is assumed; this is consistent with current cooling hole manufacturing capability [9].

$$\begin{aligned}\Delta\eta_{\text{cool}} = {} & \frac{\phi^2}{\psi}\frac{\left(\frac{\chi_r}{\cos^2\beta_2} + \frac{\chi_s}{\cos^2\alpha_3}\right)}{1 - \chi_r - \chi_s}(1 - \cos\zeta_{\text{cool}}) \\ & + \frac{\chi_r}{1 - \chi_r - \chi_s}\left(\frac{\Delta T_t}{T_{t1}}\right)^{-1}\left[\frac{T_{t3}}{T_{t1}}\left(\frac{T_{tc}}{T_{t1}}\left(\frac{T_{t2}}{T_{t1}}\right)^{-1} - 1\right) - \frac{T_{t3}}{T_{t1}}\ln\left(\frac{T_{tc}}{T_{t1}}\left(\frac{T_{t2}}{T_{t1}}\right)^{-1}\right)\right] \\ & + \frac{\chi_s}{1 - \chi_r - \chi_s}\left(\frac{\Delta T_t}{T_{t1}}\right)^{-1}\left[\left(\frac{T_{tc}}{T_{t1}} - \frac{T_{t3}}{T_{t1}}\right) - \frac{T_{t3}}{T_{t1}}\ln\left(\frac{T_{tc}}{T_{t1}}\left(\frac{T_{t3}}{T_{t1}}\right)^{-1}\right)\right]\end{aligned} \tag{D.56}$$

Appendix E

Cycle model

E.1 Gas model

Gas flows through the engine are assumed to be mixtures of perfect gases with variable $c_p(T)$: the flow is assumed to be comprised of a number of discrete species, each with it's own gas constant, enthalpy of formation, and temperature-dependent specific heat. These assumptions capture the real gas effect that are important in high temperature gas turbine cycles without excessive computational effort.

E.1.1 Gas properties

Specific heat is a function of temperature, using a cubic spline representation given tabulated $c_p(T)$ data. The gas constant R and enthalpy of formation h_F (defined at the standard temperature T_{std}) are constant for each constituent. From the tabulated $c_p(T)$ data, the enthalpy $h(T)$ and entropy complement $s'(T)$ can be calculated.

$$h(T) = h_F + \int_{T_{\text{std}}}^{T} c_p(T)dT \tag{E.1}$$

$$s'(T) = \int_{T_{\text{std}}}^{T} \frac{c_p(T)}{T}dT \tag{E.2}$$

E.1.2 Gas mixture properties

The composition of the mixture is characterized by the mass fraction vector $\vec{\alpha}$, where α_i represents the mass fraction of the i^{th} constituent. The gas properties (R, h_F, $c_p(T)$, $h(T)$, $s'(T)$) can also be represented as vectors containing the properties of each constituent. The mixture properties can then be calculated as

$$R = \sum_i \alpha_i R_i = \vec{\alpha} \cdot \vec{R} \tag{E.3}$$

$$c_p(T) = \sum_i \alpha_i c_{pi}(T) = \vec{\alpha} \cdot \vec{c_p}(T) \tag{E.4}$$

$$h(T) = \sum_i \alpha_i h_i(T) = \vec{\alpha} \cdot \vec{h}(T) \tag{E.5}$$

$$s'(T) = \sum_i \alpha_i s'_i(T) = \vec{\alpha} \cdot \vec{s'}(T) \tag{E.6}$$

E.1.3 Governing equations

Gibbs equation

$$dh = Tds + \frac{dp}{\rho} \tag{E.7}$$

Perfect gas

$$p = \rho RT \tag{E.8}$$

From definition of $h(T)$

$$dh = c_p(T)dT \tag{E.9}$$

For adiabatic work processes (e.g. in compressors and turbines), entropy generation is characterized by the polytropic efficiency.

$$Tds = c_p dT \left(1 - \frac{R}{c_p}\frac{dp}{p}\frac{T}{dT}\right) = c_p dT(1 - \eta_{\text{poly}}^{\pm 1}) \tag{E.10}$$

where the power of η_{poly} is $+1$ for compression processes (work done on fluid) and -1 for expansion processes (work extracted from fluid). Combining Equations (E.7)-(E.10), the temperature and pressure changes can be related for an adiabatic work

process given an initial state (i).

$$p(T) = p(T_i) \exp\left(\eta_{\text{poly}}^{\pm 1} \frac{s'(T) - s'(T_i)}{R}\right) \tag{E.11}$$

E.2 State change calculations

Using the described gas model and some assumed operating condition, state changes through each component of a gas turbine cycle can be calculated as a function of prescribed changes in one state variable (e.g. pressure ratio for a turbomachine, temperature change in a combustor) and some measure of loss (either a pressure loss term or the polytropic efficiency of a turbomachine).

E.2.1 Free stream quantities

Environmental conditions are characterized by a specified gas mixture $\vec{\alpha}_0$, static temperature T_0, and static pressure p_0. The stagnation quantities are calculated from a specified Mach number M_0.

$$c_{p0} = c_p(T_0) \tag{E.12}$$

$$h_0 = h(T_0) \tag{E.13}$$

$$V_0 = M_0 \sqrt{\frac{c_{p0} R_0 T_0}{c_{p0} - R_0}} \tag{E.14}$$

$$h(T_{t0}) - h_0 - \frac{1}{2} V_0^2 = 0 \quad \rightarrow \quad T_{t0} \tag{E.15}$$

$$p_{t0} = p_0 \exp\left(\eta_{\text{poly}}^{\pm 1} \frac{s'(T_{t0} - s'(T_0)}{R_0}\right) \tag{E.16}$$

$$h_{t0} = h(T_{t0}) \tag{E.17}$$

E.2.2 Fan and compressor compression

Any losses incurred before the compressor or fan face are characterized by a diffuser pressure ratio π_i.

$$T_{t2} = T_{t0} \tag{E.18}$$

$$p_{t2} = \pi_d p_{t0} \tag{E.19}$$

$$h_{t2} = h_{t0} \tag{E.20}$$

The compression calculation is the same for both the fan and compressor, differing only input pressure ratio and polytropic efficiency. The compressor calculation (2→3) is shown here, but the same procedure is also used for the fan (12→13).

$$\frac{s'(T_{t3}) - s'(T_{t2})}{R} - \frac{\ln \pi_c}{\eta} = 0 \quad \rightarrow \quad T_{t3} \tag{E.21}$$

$$p_{t3} = \pi_c p_{t2} \tag{E.22}$$

$$h_{t3} = h(T_{t3}) \tag{E.23}$$

E.2.3 Combustion

The combustion process is characterized by its initial and final temperatures, T_{t3} and T_{t4} and the fuel type, characterized by its composition $\vec{\beta}$, its temperature T_f, and a vector representing the mass fraction change in air due to combustion $\vec{\gamma}$. Conservation of energy gives the required fuel-to-air ratio f, leading to the final mass fraction vector $\vec{\alpha}_4$.

$$f = \frac{\vec{\alpha}_0 \cdot \left(\vec{h}(T_{t4}) - \vec{h}(T_{t3})\right)}{\vec{\beta} \cdot \vec{h}(T_f) - \vec{\gamma} \cdot \vec{h}(T_{t4})} \tag{E.24}$$

$$\vec{\alpha}_4 = \frac{\vec{\alpha}_0 + f\vec{\gamma}}{1 + f} \tag{E.25}$$

Any losses in the combustor are characterized by a total pressure ratio π_b.

$$p_{t4} = \pi_b p_{t3} \tag{E.26}$$

E.2.4 Mixing of two streams

The effect of cooling flow is approximated by modeling complete injection of the cooling flow into the first turbine nozzle guide vane (i.e. before any work is extracted). It is assumed that the cooling flow is at the same state and has the same composition as the compressor exit flow. The state after mixing is calculated using a constant area mixing control volume [13].

Specification of a cooling mass flow fraction ($x = \dot{m}_{\text{cool}}/\dot{m}_{\text{core}}$), and an assumed hot gas Mach number M_4 allows for calculation of the static state at the mixing plane (where static pressure p_4 is assumed constant) and a flow area ratio A_c/A_{4b}.

$$h_{t4} - h(T_4) - \frac{M_4^2 c_p(T_4) R_4 T_4}{2(c_p(T_4) - R_4)} = 0 \quad \rightarrow \quad T_4 \tag{E.27}$$

$$p_4 = p_{t4} \exp\left(\frac{s'(T_4) - s'(T_t4)}{R_4}\right) \tag{E.28}$$

$$p_4 - p_{t3} \exp\left(\frac{s'(T_c) - s'(T_{t3})}{R_3}\right) = 0 \quad \rightarrow \quad T_c \tag{E.29}$$

$$V_4 = \sqrt{2[h_{t4} - h(T_4)]} \tag{E.30}$$

$$V_c = \sqrt{2[h_{t3} - h(T_3)]} \tag{E.31}$$

$$\frac{A_c}{A_{4b}} = \left[1 + \left(\frac{1-x}{x}\right)\frac{R_4}{R_3}\frac{T_4}{T_c}\frac{V_c}{V_4}\right]^{-1} \tag{E.32}$$

Conservation of energy gives the stagnation enthalpy (and thus temperature) after mixing.

$$h_{t4b} = (1-x)h_{t4} + x h_{t3} \tag{E.33}$$

$$\vec{\alpha}_{4b} = x\vec{\alpha}_3 + (1-x)\vec{\alpha}_4 \tag{E.34}$$

$$h_{t4b} - h(T_{t4b}) = 0 \quad \rightarrow \quad T_{t4b} \tag{E.35}$$

Conservation of mass and momentum can be used calculate the static pressure, temperature, and velocity after mixing, which can be combined to calculate the stagnation pressure.

$$A = x\left(\frac{A_c}{A_{4b}}\right)^1 \frac{R_3 T_c}{V_c} + (1-x)V_4 + xV_c - \frac{R_3 T_c}{\sqrt{2[h_{t4b} - h(T_{4b})]}} - \sqrt{2[h_{t4b} - h(T_{4b})]} \tag{E.36}$$

$$A = 0 \quad \rightarrow \quad T_{4b} \tag{E.37}$$

$$V_{4b} = \sqrt{2[h_{t4b} - h(T_{4b})]} \tag{E.38}$$

$$p_{4b} = \frac{1}{x} p_4 \frac{V_c}{V_{4b}} \frac{A_c}{A_{4b}} \frac{R_{4b}}{R_3} \frac{T_{4b}}{T_c} \tag{E.39}$$

$$p_{t4b} = p_{4b} \exp\left(\frac{s'(T_{t4b}) - s'(T_{4b})}{R_{4b}}\right) \tag{E.40}$$

E.2.5 Turbine expansion

The turbine must extract enough work to power the compressor and fan, where applicable (i.e. when $\alpha \neq 0$). The enthalpy drop is calculated from the enthalpy rises across the compressor and fan, and the pressure drop can be calculated from the turbine polytropic efficiency.

$$\Delta h = \frac{(h_{t3} - h_{t2}) + \alpha(h_{t13} - h_{t12})}{1+f} \tag{E.41}$$

$$h_{t5} = h_{t4b} - \Delta h \tag{E.42}$$

$$h_{t5} - h(T_{t5}) = 0 \quad \rightarrow \quad T_{t5} \tag{E.43}$$

$$p_{t5} = p_{t4b} \exp\left(\frac{s'(T_{t5}) - s'(T_{t4b})}{\eta R}\right) \tag{E.44}$$

E.2.6 Power turbine

In the case of a gas turbine generator, useful work is produced in a power turbine after enough work to turn the compressor has been extracted. It is assumed that the pressure drops back to p_{t2} during this process; this corresponds either to a closed cycle, or an open cycle exhausting to the same reservoir from which fluid was initially

drawn.

$$p_{t8} = p_{t2} \tag{E.45}$$

$$\frac{s'(T_{t8}) - s'(T_{t5})}{\eta R} - \ln\frac{p_{t8}}{p_{t5}} = 0 \quad \rightarrow \quad T_{t8} \tag{E.46}$$

$$h_{t8} = h(T_{t8}) \tag{E.47}$$

E.2.7 Converging propelling nozzle

In the case of thrust engines, a convergent nozzle accelerates the flow exiting the fan or the turbine to provide thrust. Of interest are the pressure and velocity of the flow at the exit of the nozzle. The calculation for the core nozzle (5 →8), but the same procedure is used for the fan nozzle (13→18). Any loss incurred is characterized by total pressure ratio π_n. It is initially assumed that the pressure at the nozzle exit is equal to the ambient pressure p_0.

$$T_{t8} = T_{t5} \tag{E.48}$$

$$p_{t8} = \pi_n p_{t5} \tag{E.49}$$

$$h_{t8} = h_{t5} \tag{E.50}$$

$$p_8 = p_0 \tag{E.51}$$

$$\frac{s'(T_{t8}) - s'(T_8)}{R} - \ln\frac{p_{t8}}{p_8} = 0 \quad \rightarrow \quad T_8 \tag{E.52}$$

$$V_8 = \sqrt{2[h_{t8} - h(T_8)]} \tag{E.53}$$

$$M_8 = V_8\sqrt{\frac{c_p(T_8)RT_8}{c_p(T_8) - R}} \tag{E.54}$$

If M_8 is greater than unity, the choked condition is imposed, and the velocity and static pressure are re-calculated, as is the density, which is needed in the calculation

of specific thrust for a choked nozzle.

$$M_8 = 1 \tag{E.55}$$

$$h_{t8} - h(T_8) - \frac{M_8^2 c_p(T_8) R T_8}{2(c_p(T_8) - R)} = 0 \quad \rightarrow \quad T_8 \tag{E.56}$$

$$V_8 = \sqrt{2[h_{t8} - h(T_8)]} \tag{E.57}$$

$$p_8 = p_{t8} \exp\left(\frac{s'(T_8) - s'(T_{t8})}{R}\right) \tag{E.58}$$

$$\rho_8 = \frac{p_8}{R T_8} \tag{E.59}$$

E.3 Performance calculation

E.3.1 Thermal efficiency

For the case of a gas turbine generator, the performance metric considered is the thermal efficiency, equal to the rate of work extraction in the power turbine divided by the rate of energy addition in the fuel.

$$\eta_{th} = \frac{h_{t5} - h_{t8}}{f(LHV)} \tag{E.60}$$

E.3.2 Thrust-specific fuel consumption

For the case of a thrust engine, the performance metric considered is the thrust-specific fuel consumption, a function of the fuel-to-air ratio, bypass ratio, and the static pressures and velocities exiting the thrust-producing nozzles and at the free stream conditions.

$$F_{sp} = (1+f)V_8 - V_0 + \frac{p_8 - p_0}{\rho_8 V_8} + \alpha\left[V_{18} - V_0 + \frac{p_{18} - p_0}{\rho_{18} V_{18}}\right] \tag{E.61}$$

$$TSFC = \frac{f}{F_{sp}} \tag{E.62}$$

Bibliography

[1] Bejan, A., *Advanced Engineering Thermodynamics*, 3rd ed., John Wiley & Sons, Inc., 2006.

[2] Benzakein, M. J., "Propulsion Strategy for the 21st Century: A Vision Into the Future," 2001.

[3] Clark, J. M., Horlock, J. H., "Availability and Propulsion," *Journal of Mechanical Engineering Science*, Vol. 17, No. 4, pp. 223-232, 1974.

[4] Cumpsty, N. A., *Compressor Aerodynamics*, 1st ed., Longman Group UK Ltd., 1989.

[5] Cumpsty, N. A., *Jet Propulsion: A Simple Guide to the Aerodynamic and Thermodynamic Design and Performance of Jet Engines*, 2nd ed., Cambridge University Press, 2003.

[6] Denton, J. D., "Axial Turbine Aerodynamic Design," Cambridge Turbomachinery Course Notes.

[7] Denton, J. D., "Loss Mechanisms in Turbomachines - The 1993 IGTI Scholar Lecture," *Journal of Turbomachinery*, Vol. 115, pp. 621-656, Oct. 1993.

[8] Dickens, T., Day, I., "The Design of Highly Loaded Axial Compressors," *Proceedings of ASME Turbo Expo 2009: Power for Land Sea and Air*, 2009.

[9] Downs, J. P., Landis, K. K., "Turbine Cooling Systems Design - Past, Present, and Future," *Proceedings of ASME Turbo Expo 2009: Power for Land Sea and Air*, 2009.

[10] Drela, M., "Power Balance in Aerodynamic Flows," *AIAA Journal*, Vol. 47, No. 7, pp. 1761-1771, July 2009.

[11] Drela, M., Giles, M. B., "Viscous-Inviscid Analysis of Transonic and Low Reynolds Number Airfoils," *AIAA Journal*, Vol. 25, No. 10, pp. 1347-1355, Oct. 1987.

[12] Greitzer, E. M., "N+3 Aircraft Concept Design and Trade Studies," Technical report, MIT, 2010.

[13] Greitzer, E. M., Tan, C. S., Graf, M. B., *Internal Flow: Concepts and Applications*, Cambridge University Press, 2004.

[14] Guha, A., "Optimisation of Aero Gas Turbine Engines," *The Aeronautical Journal*, pp. 345-358, July 2001.

[15] Guha, A., "Performance and Optimization of Gas Turbines with Real Gas Effects," *Proceedings Institution of Mechanical Engineers*, Vol. 215, Part A, pp. 507-512, 2001.

[16] Gunston, B. (ed.), *Jane's Aero-Engines*, Jane's Information Group Inc., 2007.

[17] Halstead, D. H., Wisler, D. C., Okiishi, T. H., Walker, H. P., Hodson, H. P., Shin, H.-W., "Boundary Layer Development in Axial Compressors and Turbines: Part 1 of 4 - Composite Picture," *Journal of Turbomacinery*, Vol. 119, pp. 114-127, Jan. 1997.

[18] Haywood, R. W., *Analysis of Engineering Cycles*, Pergamon Press, 1991.

[19] Hodson, H. P., Howell, R. J., "Bladerow Interactions, Transition, and High-Lift Aerofoils in Low-Pressure Turbines," *Annual Review of Fluid Mechanics*, Vol. 37, pp. 71-98, 2005.

[20] Horlock, J. H., "The Rational Efficiency of Power Plants and Their Components," *Journal of Engineering for Gas Turbines and Power*, Vol. 114, pp. 603-611, Oct. 1992.

[21] Horlock, J. H., "The Basic Thermodynamics of Turbine Cooling," *Journal of Turbomachinery*, Vol. 123, pp. 583-592, July 2001.

[22] Horlock, J. H., Watson, D. T., Jones, T. V., "Limitations on Gas Turbine Performance Imposed by Large Turbine Cooling Flows," *Hournal of Engineering for Gas Turbines and Power*, Vol. 123, pp. 487-494, July 2001.

[23] Horlock, J. H., "Thermodynamic Availability and Propulsion," *AIAA ISABE*, 1999.

[24] Keenan, J. H., *Thermodynamics*, John Wiley & Sons, Inc., 1947.

[25] Kerrebrock, J. L., *Aircraft Engines and Gas Turbines*, 2nd ed., MIT Pres, 1992.

[26] Koch, C. C., Smith, L. H., "Loss Sources and Magnitudes in Axial-Flow Compressors," *Journal of Propulsion and Power*, Vol. 20, No. 4, pp. 577-595, Aug. 2004.

[27] Koff, B. L., "Gas Turbine Technology Evolution: A Designer's Perspective," *Journal of Propulsion and Power*, Vol. 20, No. 4, pp. 577-595, Aug. 2004.

[28] Kotas, T. J., *The Exergy Method of Thermal Plant Analysis*, Butterworths, 1989.

[29] Lieblein S., Stockman, N. O., "Compressibility Correction for Internal Flow Solutions," *AIAA Journal of Aircraft*, Vol. 9, No. 4, pp. 312-313, Apr. 1972.

[30] Ludwig, L. P., "Gas Path Sealing in Turbine Engines," Paper 1, AGARD Specialists Meeting "Seal Technology in Gas Turbine Engines," AGARD-CP-237, Aug. 1978.

[31] Mattingly, J. D., *Elements of Propulsion: Gas Turbines and Rockets*, AIAA, 2006.

[32] Mitsubish Heavy Inustries, Ltd., "Gas Turbine Development," Company website, `http://www.mhi.co.jp/en/products/detail/gas_turbine_development.html`.

[33] Moran, M. H., *Availability Analysis: A Guide to Efficient Energy Use*, ASME Press, 1989.

[34] Nelder, J. A., Mead, R., "A Simplex Method for Function Minimization," *The Computer Journal*, 1965.

[35] Plas, A. P., Sargeant, M. A., Madani, V., Crichton, D., Greitzer, E. M., Hynes, T. P., Hall, C. A., "Performance of a Boundary Layer Ingesting (BLI) Propulsion System," *45th AIAA Aerospace Sciences Meeting and Exhibit*, Jan. 2007.

[36] Press, W. H., Teukolsky, S. A., Vetterling, W. T., Flannery, B. P., *Numerical Reipes in FORTRAN: The Art of Scientific Computing*, 2nd ed., Cambridge University Press, 1992.

[37] Saravanamutto, H. I. H., Rogers, G. F. C., Cohen, H., *Gas Turbine Theory*, 5th ed., Prentice Hall, 2001.

[38] Schlichting, H., Gerste, K., *Boundary Layer Theory*, 8th ed., Springer-Verlag, 2000.

[39] Smith, L. H., "Wake Dispersion in Turbomachines," *ASME Journal of Basic Engineering*, Vol. 88, pp. 688-690, 1966.

[40] Storer, J. A., Cumpsty, N. A., "Tip Leakage Flow in Axial Compressors," *Journal of Turbomachinery*, Vol. 113, pp. 357-365, Oct. 1989.

[41] Storer, J. A., Cumpsty, N. A., "An Approximate Analysis and Prediction Method for Tip Clearance Loss in Axial Compressors," *Journal of Turbomachinery*, Vol. 116, pp. 648-656, Oct. 1994.

[42] Wennerstrom, A. J., "Low Aspect Ratio Axial Compressors: Why and What it Means," *Journal of Turbomachinery*, Vol. 111, pp. 357-365, Oct. 1989.

[43] Wilcock, R. C., Young, J. B., Horlock, J. H., "The Effect of Turbine Blade Cooling on the Cycle Efficiency of Gas Turbine Power Cycles," *Journal of Engineering for Gas Turbines and Power*, Vol. 127, pp. 109-120, Jan. 2005.

[44] Wisler, D. C., "Advanced Compressor and Fan Systems," Lecture notes.

[45] Wright, P. I., Miller, D. C., "An Improved Compressor Performance Prediction Model," *European Conference of Turbomachinery: Latest Developments in a Changing Scene*, IMechI, 1991.

[46] Yaras, M. I., Sjolander, S. A., "Losses in the Tip-Leakage Flow of a Planar Cascade of Turbine Blades," Paper 20, AGARD Specialists Meeting "Secondary Flows in Turbomachines," AGARD-CP-469, Feb. 1990.

[47] Yaras, M. I., Sjolander, S. A., "Prediction of Tip-Leakage Losses in Axial Turbines," *Journal of Turbomachinery*, Vol. 114, pp. 204-210, Jan. 1992.

[48] Young, J. B., Horlock, J. H., "Defining the Efficiency of a Cooled Turbine," *Journal of Turbomachinery*, Vol. 128, pp. 658-667, Oct. 2006.

[49] Young, J. B., Wilcock, R. C., "Modeling the Air-Cooled Gas Turbine: Part 1 - General Thermodynamics," *Journal of Turbomachinery*, Vol. 124, pp. 207-213, Apr. 2002.

[50] Young, J. B., Wilcock, R. C., "Modeling the Air-Cooled Gas Turbine: Part 2 - Coolant Flows and Losses," *Journal of Turbomachinery*, Vol. 124, pp. 207-213, Apr. 2002.